RECORD
2023/12

SYSTEMATIC CLASSIFICATION OF YILGARN CRATON GRANITIC ROCKS

JR Lowrey, RH Smithies, DC Champion and KF Cassidy

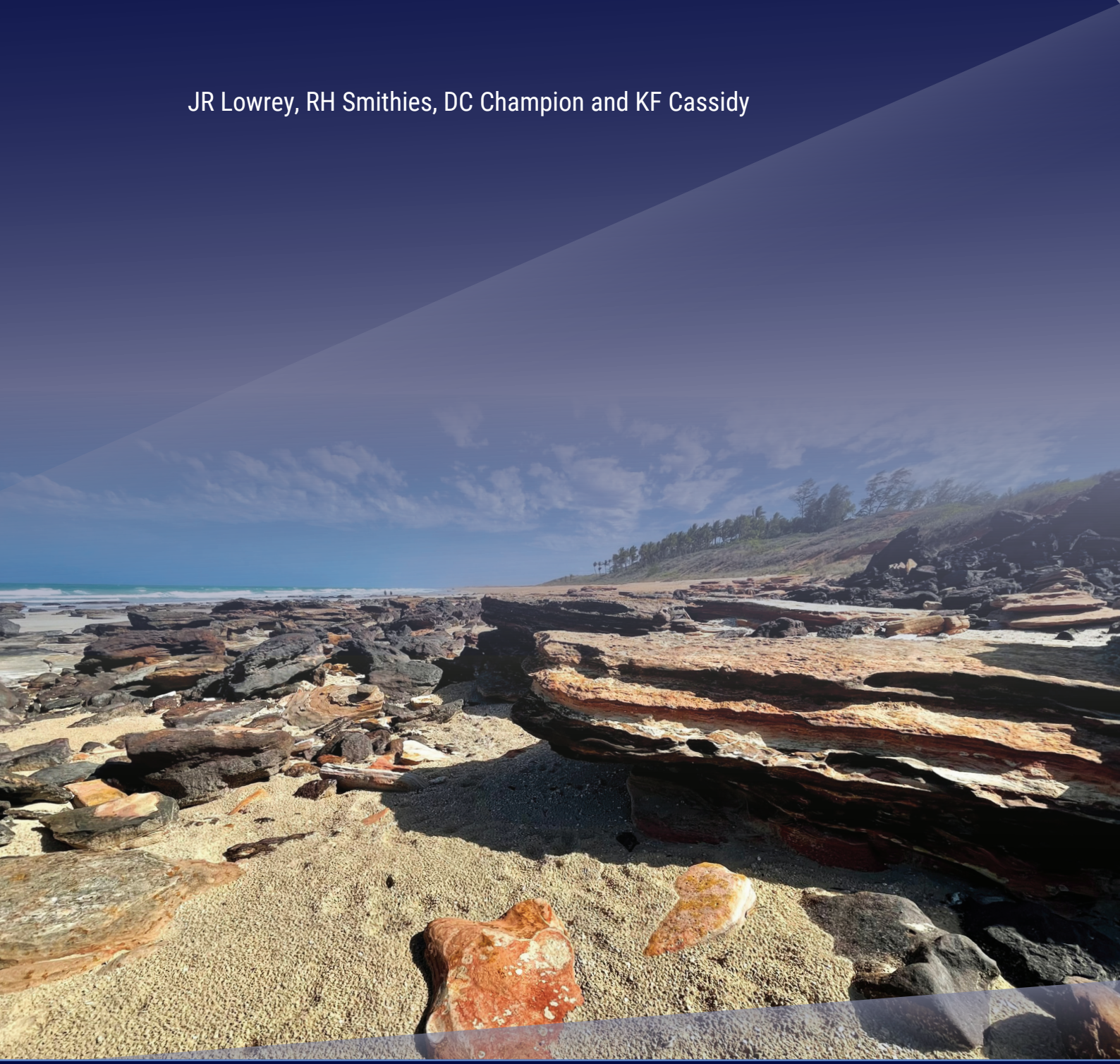

Government of Western Australia
Department of Mines, Industry Regulation and Safety

Geological Survey of Western Australia

Government of **Western Australia**
Department of **Mines, Industry Regulation and Safety**

RECORD 2023/12

SYSTEMATIC CLASSIFICATION OF YILGARN CRATON GRANITIC ROCKS

JR Lowrey, RH Smithies, DC Champion[1] and KF Cassidy[2]

1 Geoscience Australia, 1010 Jerrabomberra Ave, Symonston ACT 2609, Australia
2 Bare Rock Geological Services, Fremantle WA 6160, Australia

PERTH 2023

Geological Survey of Western Australia

MINISTER FOR MINES AND PETROLEUM
Hon Bill Johnston MLA

DIRECTOR GENERAL, DEPARTMENT OF MINES, INDUSTRY REGULATION AND SAFETY
Richard Sellers

EXECUTIVE DIRECTOR, GEOLOGICAL SURVEY AND RESOURCE STRATEGY
Michele Spencer

REFERENCE
The recommended reference for this publication is:
Lowrey, JR, Smithies, RH, Champion, DC and Cassidy, KF 2023, Systematic classification of Yilgarn Craton granitic rocks: Geological Survey of Western Australia, Record 2023/12, 27p.

ISBN 978-1-74168-016-4
ISSN 2204-4345

Grid references in this publication refer to the Geocentric Datum of Australia 1994 (GDA94). Locations mentioned in the text are referenced using Map Grid Australia (MGA) coordinates, Zone 50. All locations are quoted to at least the nearest 100 m.

Published 2023 by the Geological Survey of Western Australia
This Record is published in digital format (PDF) and is available online at <www.dmirs.wa.gov.au/GSWApublications>.

Further details of geoscience products are available from:
First Floor Counter
Department of Mines, Industry Regulation and Safety
100 Plain Street
EAST PERTH WESTERN AUSTRALIA 6004
Telephone: +61 8 9222 3459 Email: publications@dmirs.wa.gov.au
www.dmirs.wa.gov.au/GSWApublications

Cover image: Episodic tides discharge sediments along a rocky shoreline at Cable Beach, Broome. Photo by Robin Bower

Contents

Figures

Appendices

Available with the PDF online as an accompanying digital resource

1. MS Excel Workbook containing Yilgarn Granite Project geochemical dataset (Lowrey et al., 2022) with
2. classification workflow calculations
3. MS Excel Workbook containing mixed acid ICP-MS data from the Yilgarn Granite Project geochemical dataset (Lowrey et al., 2022) with modified classification workflow calculations
4. ioGAS calculation file for classification of Yilgarn Craton granitic rocks

Systematic classification of Yilgarn Craton granitic rocks

JR Lowrey, RH Smithies, DC Champion[1] and KF Cassidy[2]

Abstract

This study presents recent work conducted under the Yilgarn Granite Project (an initiative of the State Government of Western Australia's Exploration Incentive Scheme) to produce a systematic classification scheme for granitic rocks of the Yilgarn Craton. The classification scheme is based on a considerable body of previous work, primarily by Geoscience Australia, on the petrogenesis and distribution of Yilgarn granites. The studies of Champion and Sheraton (1997) and Champion and Cassidy (2002), though heavily reliant on geochemical data, were also mindful of available petrography work and of local field relationships in defining five major granitic groups, distributed across the craton. The present study aims to recreate those classifications using whole rock geochemical data alone – mainly high-quality re-assays of Geoscience Australia's Yilgarn granite collection (now housed with the GSWA). Although the methodology of this study enforces hard compositional boundaries between the granite groups, in reality, the compositional boundaries between the five granite groups are transitional in nature, which results in a small, but acceptable, number of discrepancies with the original classifications. The clear advantage of this approach, however, is the ability to rapidly classify granitic rocks, with a high level of confidence, where additional geological context is limited. We expect this approach, and the supplementary files that enable users to rapidly classify their own datasets, to be of use to mineral explorers where identifying specific classes of granitic rocks is important within a mineral system context – such as the relationship between sanukitoids and gold mineralization in the Yilgarn Craton. This work is also expected to improve the efficiency of regional geological mapping studies in the Yilgarn Craton, particularly in poorly understood study areas.

KEYWORDS: Archean, granite classification, whole-rock geochemistry, Yilgarn Craton

Introduction

The Yilgarn Granite Project is an initiative under the State Government Exploration Incentive Scheme that aims to provide complete and detailed coverage of the Yilgarn Craton in terms of modern, high-quality, major and trace element data on felsic intrusive rocks. The Project aims also include identification of potential proxies for magma source compositions, melting conditions and fertility for precious metal and strategic mineral deposits. As data is accumulated, the Project will provide interpretation (digital data, GIS layers, reports) that attempts to place these data within the context of crustal scale structure, source regions and economic mineral fertility.

The purpose of this Record is to present recent efforts to systematically classify the chemical characteristics of Yilgarn Craton granitic rocks by methods that can be utilized by explorers and geoscientists to classify samples from their own datasets. This new scheme builds on a widely used classification scheme for Yilgarn Craton granites (Champion and Sheraton, 1997; Champion and Cassidy, 2002) that was based on a considerable body of previous work, primarily by Geoscience Australia (GA), on the petrogenesis and distribution of Yilgarn granites.

The data presented in figures herein and included in Appendix 1 are from the most recent Yilgarn Granite Project data release (Lowrey et al., 2022). The vast majority of these data were derived from reanalysing archived materials, mainly from GA's Yilgarn granite collection (now housed with the Geological Survey of Western Australia; GSWA), using the best whole-rock chemical assay methods commercially available. Utilizing a single laboratory and sample workflow eliminates the potential for discrepancies in precision and accuracy due to differences in analytical methodology. Major element compositions for the vast majority of GA's Yilgarn granite collection were considered broadly equivalent to present-day methods and were not repeated, except where GA's database did not contain original analyses. For most reported trace elements, detection levels have lowered by an order of magnitude or more compared to the original methods, and we therefore expect this reanalysed data to be subject to a commensurate improvement in precision. The

1 Geoscience Australia, 1010 Jerrabomberra Ave, Symonston ACT 2609

2 Bare Rock Geological Services, Fremantle WA 6160

dataset also includes a smaller number of newly collected granitic samples and samples from the GSWA's archive, derived from outcrop and drillcores across the Yilgarn Craton. These latter samples have all been analysed or reanalysed following the same procedures as the GA samples.

Sample selection and analytical techniques

Dataset content

The dataset presented here (n=3028; Appendix 1) contains only those samples collected or reanalysed specifically for the Yilgarn Granite Project. Other data produced by the GSWA, and various universities and research organizations, are available in published literature or in publicly available online datasets (e.g. GSWA Geochemistry [WACHEM]; www.dmp.wa.gov.au/geochem). The dataset presented here includes whole-rock major and trace element data primarily covering granitic (or metagranitic) lithologies including high-level (subvolcanic) felsic intrusive rocks (commonly referred to as 'felsic porphyry'). It also includes some mafic igneous rocks, such as lamprophyres and quartz-gabbroic rocks, where a comagmatic relationship with felsic derivatives can be established or realistically inferred. These mafic rocks are not included within the classification scheme outlined here; they are automatically excluded from the classification process by screens that filter based on silica content.

The vast majority of analyses reported here are re-assays of powders from GA's granite dataset (n=2829). The dataset also contains recent geochemical data for 199 samples, including samples collected from diamond drillcores and outcrops for current GSWA projects (n=93), samples from the GSWA sample archive (n=85), and samples from the Curtin University sample archive (n=21). The list of drillcores that were sampled is provided in Appendix 1 (under the spreadsheet labelled 'DDH details'). This list includes details of the location, length and average or initial orientation of the drillholes. Where orientation details are unavailable, the drillhole is assumed to be vertical. The sampling interval (length/depth in the relevant core) is noted for all recent drillcore samples. Each sample is accompanied by a geological description (Lithology, Field description and Field notes). These are largely uncorrected or unedited notes made at the time of sampling.

Most samples in GA's Yilgarn granite dataset have ferric and ferrous proportions of iron reported. Ferrous iron (Fe^{2+}; reported as FeO) was determined by titration and then used to calculate Fe^{3+} by the difference from total Fe as measured by X-ray fluorescence spectrometry (XRF). For all new samples, ferrous and ferric iron proportions were not determined, and all iron (total) is reported in the ferric state, denoted as Fe_2O_3T. All major element concentrations and totals are calculated and reported both considering and ignoring analytical loss on ignition (LOI), the prefix 'a' (e.g. $aSiO_2$) denoting a concentration recalculated volatile free.

Analytical methodology

Trace element concentrations for all analyses reported here were measured at a single commercial laboratory (Australian Laboratory Services [ALS] Global Pty Ltd) employing a single set of analytical procedures, outlined below. This approach minimizes the potential for any variation in the dataset potentially attributable to variations in analytical procedure. Major element and LOI assays for new samples were also measured at ALS, whereas for the reanalysis of GA's granite collection, it was decided that since the existing major element concentrations were determined using comparable methods and of similar quality to those being offered by commercial laboratories, this component of the analysis suite would not be repeated.

New samples collected for the purpose of this study were visibly inspected and any weathering or excessive vein material was removed. Each sample was crushed by the GSWA using a plate jaw crusher and splitter and milled by ALS using a low-Cr steel mill to produce a pulp with a nominal particle size of 85% <75 µm. A quartz-feldspar aggregate material containing below detection level concentrations of transition and precious metals was milled between each sample to scrub any remaining pulp residue from the previous sample. Representative pulp aliquots were analysed for 14 elements as major and minor oxide element components (of which we report 11; BaO, Cr_2O_3 and SrO are instead reported here as trace elements [Ba, Cr and Sr]), mass LOI and 60 elements as trace elements. Major and minor elements were determined by mixing a 0.66 g aliquot of sample with lithium borate flux ($LiBO_2$, LiB_4O_7 and $LiNO_3$) in a 1:10 ratio, and then fusing the mixture at 1025 °C and pouring it into a platinum mold. The resulting disk was analysed by XRF (ALS method ME-XRF26). LOI was determined by thermogravimetric analysis (ALS method ME-GRA05). For trace elements associated with minerals that are not fully dissolved by mixed acid digests alone (i.e. Cr, V, Cs, Rb, Ba, Sr, Th, U, Nb, Zr, Hf, Y, La, Ce, Pr, Nd, Sm, Eu, Gd, Tb, Dy, Ho, Er, Tm, Yb and Lu), an aliquot of the sample was mixed with lithium borate flux and fused, then digested in acid and analysed by inductively coupled plasma mass spectroscopy (ICP-MS; ALS method ME-MS81). For the remaining trace elements (Ag, As, Be, Bi, Cd, Co, Cu, Ge, In, Li, Mo, Ni, Pb, Re, Sb, Sc, Se, Te, Tl and Zn); that is, predominantly transition metals, a 0.25 g aliquot of sample was digested with a mixture of concentrated acids ($HClO_4$, HNO_3 and HF), heated at 185 °C until incipient dryness, then leached with 50% HCl and diluted to volume with weak HCl, then analysed by ICP-MS and inductively coupled plasma atomic emission spectroscopy (ALS method ME-MS61L).

Data quality was monitored by 'blind' insertion of sample duplicates (i.e. a second aliquot of pulp or finely crushed material) at a rate of 1 per 10 unknown samples, as well as the GSWA's internal reference materials and certified reference materials (OREAS 24b; <www.ore.com.au>), also inserted at a rate of 1 per 10 unknown samples. The laboratory also conducted repeat analyses of samples, variably certified reference materials and blanks. Accuracy and precision were assessed using analyses of certified

reference sample OREAS 24b that were submitted together with Yilgarn Granite Project samples (10 analyses by ME-XRF26, 83 analyses by ME-MS81, 89 analyses by ME-MS61L). For analytes where the concentration is at least 10 times the lower level of detection (all analytes except Ag, Cd, Cl, In, Re, Sb, Te, Tl and W), a measure of accuracy is provided by the agreement between the average determined value and the certified value according to half absolute relative difference (HARD); that is, (analysis1 – analysis2)/(analysis1 + analysis2) (Stanley and Lawie, 2007). The average of measured major and minor element concentrations agree to within 2 HARD% of their certified values. The average of measured trace element concentrations agree to within 5 HARD% of their certified values, except for Be (7 HARD%). In terms of precision, the relative standard deviation (RSD), or covariance, for analysis of OREAS 24b is ≤3% RSD for major and minor elements and ≤10% RSD for most trace elements. The exceptions are Ag, Bi, In, Se, Sn and W (19%, 37%, 25%, 11%, 11% and 11% RSD respectively). Similar levels of agreement were found for the GSWA's reference materials (granodiorite GRD-1 and basalt BB1) and between duplicate pair samples. All blank values were less than three times the lower level of detection.

Granite classification scheme

Granitic rocks of the Yilgarn Craton have traditionally been divided based on the classification scheme of Champion and Sheraton (1997), modified by Champion and Cassidy (2002). The present study places a series of clear compositional boundaries on the various granite compositional groups identified within these schemes. It also expands the classifications by adding additional proxies reflecting variations in source compositions and melting conditions, and it provides a workflow that systematically allows each group of felsic rocks to be isolated. Additional sub-classification based on the work of Smithies et al. (2018), using K_2O/Na_2O and Sr/Y as proxies reflecting variations in source compositions and melting conditions respectively, are placed on several of the granite compositional groups.

In the process of devising a compositional scheme for separating the various granitic compositional groups, an appreciation is immediately gained of the continuous nature of the bulk of the granite compositional data. This emphasizes a large degree of overlap in the range and influence of magma-forming processes and source compositions. Examples representing one specific tectonomagmatic process or a single 'pure' source are a minority. The geochemistry for the great majority of samples shows the effects of a range of competing processes, and the petrogenetic ambiguities associated with this are an unfortunate reality of granite studies. The result is that some of the compositional boundaries used in the classification scheme are partly arbitrary, although natural low points in data density distribution are exploited where possible. Other boundaries, for example the Mg-number [the ratio of Mg to Fe in molar terms (MgO wt% / 40.3) / (MgO wt% / 40.32 + (2 * (Fe_2O_3 wt% / 159))) * 100)], Cr and Ni ranges defining sanukitoids (Shirey and Hanson, 1984; Stern et al., 1989; Martin et al., 2005) or Sr/Y and K_2O/Na_2O ranges expected of tonalite–trondjhemite–granodiorite (TTG) series granitic rocks (encompassed within the High-Ca granite group of Champion and Sheraton, 1997 [Martin et al., 2005; Moyen and Martin, 2012; Smithies et al., 2018]), reflect previously defined compositional fields. However, many of the broader compositional boundaries and fields are based on comparisons with compositional fields in the earlier classified data from Champion and Sheraton (1997) and Champion and Cassidy (2002), in which a strong emphasis was also placed on local field relationships and on available petrological data (as per both geochemical and petrographic classification keys in Champion and Cassidy, 2002). Users of this classification scheme must remain cognizant of these limitations – specifically, that it is using geochemical data alone to place specific names on rocks that have evolved within complex geological systems. Ultimately, it is the user's responsibility to assess results, particularly unexpected results, within the context of other available geological data; a single sample classified as a Syenite within a sea of Low-Ca granites, for example, deserves further scrutiny.

Champion and Sheratons' High-Ca granite group, reflecting partial melts of a hydrated mafic crustal source, is here split between high- and low-Sr/Y subdivisions reflecting enriched and/or deep (i.e. > ~40 km) sources (Sr/Y > 40) or unenriched and/or shallow sources (Sr/Y <40; <~40km). High-Ca granites (both high- and low-Sr/Y) were also split into 'very sodic' (Na+), 'sodic' (Na) and 'potassic' (K) subgroups based on K_2O/Na_2O ranges of 0–0.6, >0.6–1.0 and >1.0 respectively, reflecting the amount of reworked crustal material contributing K to otherwise K-poor 'basaltic' bulk source compositions and/or reflecting decreasing degrees of partial melting.

Low-Ca granite – ranging to higher SiO_2, K_2O, and incompatible trace element concentrations than most High-Ca granites – reflect re-melting of a bulk source on average more evolved (i.e. reworked High-Ca granite ± mafic crust ± sedimentary rocks) and dryer than the source for High-Ca granites, and typically at higher temperatures. A subclass of Low-Ca granites with high TiO_2 and P_2O_5 contents, locally including orthopyroxene-bearing examples (i.e. charnockites), reflects high temperature crustal melting of a dry and refractory source (Smithies et al., 2021). This study refers to these as 'Low-Ca (high-Ti) granites'.

Champion and Sheraton's 'Mafic granite' group was subdivided based on proxies for degree of source evolution and source enrichment. Thus, this group was divided into:

- Sanukitoids: high Mg-number (Mg-number >50 at 60 wt% SiO_2), high Cr and Ni (at 60 wt% SiO_2, Cr >80 ppm, Ni >50 ppm) and high Sr/Y >30. Note that this definition is considerably less restrictive than the original definition for sanukitoid and is based on the observation that many discrete Mafic granite bodies containing a large number of samples meeting the strict definition (at 60 wt% SiO_2 Mg-number >60, Cr and Ni >100 ppm – Shirey and Hanson, 1984; Stern et al., 1989) also show a range to these lower values
- Sanukitoid-like rocks: low Mg-number (Mg-number <50 at 60 wt% SiO_2), low Cr and Ni (at 60 wt% SiO_2, Cr >80 ppm, Ni >50 ppm) and high Sr/Y >30
- Diorites: Sr/Y <30.

Champion and Cassidy (2002) adopted a low- and high-large ion lithophile element (LILE) subdivision of the Mafic granite group, acknowledging a broad continuum between these subdivisions. The high-LILE subdivision and low-LILE subdivisions broadly encompass Sanukitoid and Diorite, respectively, as defined here, whereas the Sanukitoid-like rocks encompass much of the overlap between them.

Syenites, High-high field strength element (HFSE) granites as well as all groups previously encompassed under the Mafic granite classification are also divided here into K-rich and Na-rich based on a K_2O/Na_2O boundary of 0.6.

Before outlining the classification procedure, caveats regarding SiO_2 and gneissic rocks need to be addressed. For datasets where Si has not been determined, the best proxy for SiO_2 wt%, at least for Yilgarn Craton felsic data, is obtained by subtracting LOI, Al_2O_3, TiO_2, MgO, Fe_2O_3, MnO, Na_2O, K_2O and P_2O_5 (in wt%) from 100 (100%). Expected errors are typically around ±2 wt% of the SiO_2 value determined by XRF analysis. If Na_2O has also not been determined, an assumed value of Na_2O = 2.0 wt% can be used, although this broadly reflects the average Na_2O content across the entire dataset and will result in additional errors up to ±3 wt% for highly sodic rocks.

Regarding gneissic rocks, geochemical classification schemes for igneous rocks are typically based on the assumption that the analysis largely reflects a snapshot of a single magma (liquid ± minimal crystals) composition. This assumption is generally acceptable for relatively undeformed (enclave-free and homogeneous) rocks but becomes increasingly questionable as the cumulate mineral or enclave content of a rock increases. It is typically not a safe assumption to make for banded and gneissic rocks where the banding may represent transposed exogenous potentially unrelated rocks (e.g. enclaves, dykes, sills). However, early studies (e.g. Champion and Sheraton, 1997) specifically compared compositions of gneissic and variably deformed rocks with undeformed granites of the Yilgarn Craton and showed that compositions were largely comparable regardless of degree of deformation and metamorphism. Despite this, classification of strongly banded (or heterogeneous) rocks should be undertaken with caution.

Classification procedure

The classification procedure developed here is based on analytical methods that ideally ensure that the results reflect full dissolution of all mineral constituents of a sample into the analysed aliquot; that is, they include a process that fuses the sample, breaking down mineral structures and forming a homogeneous glass, prior to digestion and (or) analysis. The classification procedure also requires a full suite of major element analyses, including SiO_2 and LOI. Geochemical analytical packages commonly employed by the mineral exploration industry typically do not include SiO_2 or LOI, and additionally rely on four-acid digest processes that do not include a fusion step and therefore do not ensure full dissolution of a range of trace elements critical to our classification procedure. Furthermore, determination of major elements by mixed acid digests may yield lower recoveries of certain elements (e.g. Al_2O_3, CaO and K_2O) than traditional XRF methods. As a result, in order to follow this classification procedure, mineral explorers will likely need to acquire a representative dataset that complies with these amounts of more appropriate analytical data.

As an alternative, we have additionally developed a modified classification procedure using a typical mineral exploration-focused (mixed acid ICP-MS) dataset (Appendix 2) that attempts to mirror the results from the primary classification procedure below. This mixed acid-only classification process should be considered a 'work in progress' and currently only reproduces 'correct' classifications in approximately 91% of cases, with the main source of errors coming from incorrect assignment of Low-Ca granites into the High-Ca granite group and vice versa and of High-Ca granites into the Mafic granite group and vice versa.

The MS Excel workbooks in Appendices 1 and 2 include templates for users to insert their own data that will populate calculation fields and assign a granite class according to the workflow that is chosen (i.e. the comprehensive analytical suite classification workflow described below [Appendix 1] or, the modified mixed acid digest only classification workflow [Appendix 2]). The calculations used in the comprehensive analytical suite classification workflow are also provided as an ioGAS calculation (.xml) file (Appendix 3), the use of which requires the user to copy the .xml file into their ioGAS calculation folder. Afterwards, the calculation can then be accessed in ioGAS from the Calculation>User menu (note that for the calculations to work, all analytes referred to in the workflow below must be present in the user's dataset; for more information see the ioGAS Help menu).

The classification process that follows is intended to be undertaken in a systematic process, completing each step in numerical order.

Step 1. Screening the dataset for samples with inappropriate (mafic) or altered compositions

The dataset (Fig. 1) is first screened for samples with compositions that have likely been significantly altered from their primary (igneous) compositions during metamorphic, hydrothermal, or low-temperature alteration processes. There are six data screening criteria that are consolidated into a single calculation and included in the appendices in MS Excel (Appendix 1) and ioGAS (Appendix 3) formats; an explanation for each of the criteria used to screen the dataset follows below.

Approximately 20% of the dataset used here is excluded through application of filters, and approximately half of these are excluded based on silica content and reflect mafic igneous compositions rather than altered rocks. In near-mine or other potentially highly altered settings, the alteration filters decsribed below may still exclude an unacceptably high proportion of the dataset. Even relatively moderate degrees of albitization, for example, can significantly elevate the Aluminium Saturation Index (ASI). If this is the case, the user may choose to alter the tolerances set here, such as for ASI and LOI. For example, reducing the ASI and LOI cutoffs by 0.4 and 2.0 wt%, respectively, in our database successfully classifies 30% of the previously unclassifiable high silica (>57.5 wt% SiO_2) data, although with greater uncertainty.

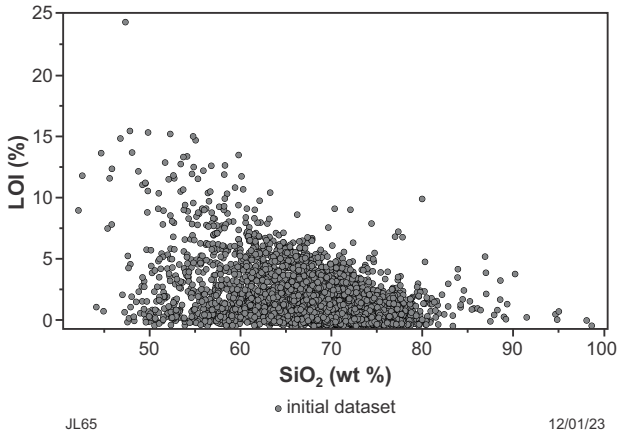

Figure 1. SiO_2 vs loss on ignition (LOI) for the entire (unscreened) dataset

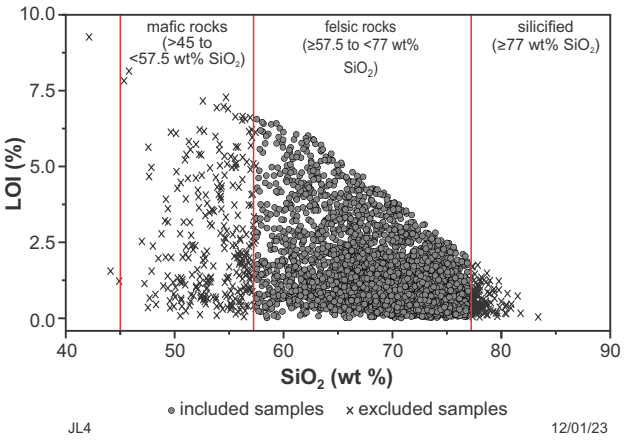

Figure 3. SiO_2 vs LOI showing samples excluded based on low- or high-SiO_2 concentrations and samples that remain in the sample pool

1.1 SiO_2 vs LOI

On a plot of SiO_2 vs LOI (Fig. 2), samples that plot to the right of a line with slope $y = -0.1714x + 16.714$ *or* to the right of a line with a slope of $y = -0.2759x + 23.241$ are excluded from the dataset for having unacceptably high LOI, interpreted here to reflect unacceptably high degrees of low-temperature (hydration and carbonation) alteration.

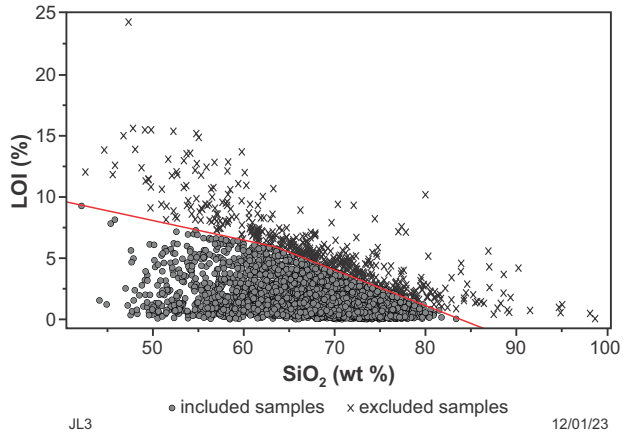

Figure 2. SiO_2 vs LOI showing samples excluded in Step 1.1 for their high LOI (black crosses) and samples that remain in the sample pool (grey circles)

1.2 Excluding non-felsic lithologies by SiO_2 concentration

Samples containing <57.5 wt% SiO_2 (i.e. mafic lithologies) *or* >77 wt% SiO_2 (i.e. silicified rocks) are excluded from the dataset (Fig. 3).

1.3 SiO_2 vs MgO

On a plot of SiO_2 wt% vs MgO wt% (Fig. 4), samples that plot to the right of a line with a slope of $y = -0.5645x + 45.403$ are excluded because their high-MgO concentrations are suspected to reflect contamination by mafic or ultramafic crust or partial mafic cumulate affects, and in some cases probably alteration.

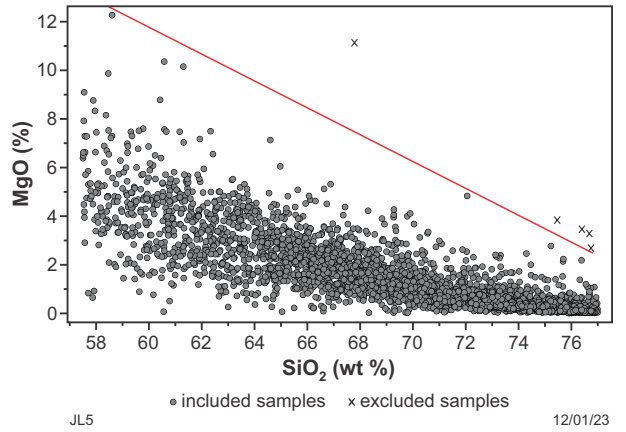

Figure 4. SiO_2 vs MgO showing samples excluded based on their high-MgO concentrations and samples that remain in the sample pool

1.4 SiO_2 vs molar $Al_2O_3/(Na_2O + K_2O + CaO)$

On a plot of SiO_2 wt% vs Aluminium Saturation Index (ASI); that is, molar $Al_2O_3/(Na_2O + K_2O + CaO)$ (Fig. 5), samples that plot on the high-ASI side of a line with a slope of $y = 0.0141x + 0.1172$ are excluded as they are interpreted here to reflect high degrees of alteration.

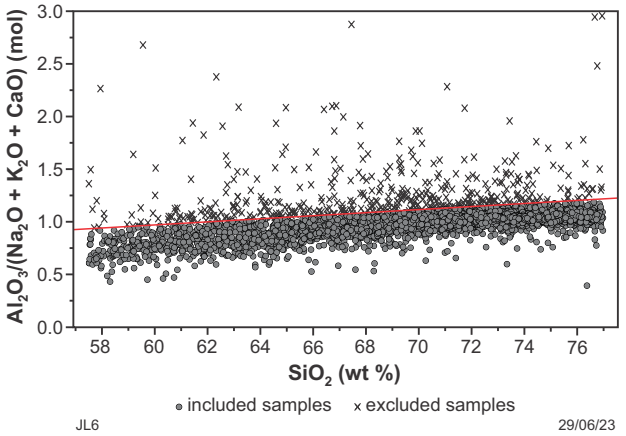

Figure 5. SiO_2 vs molar $Al_2O_3/(Na_2O + K_2O + CaO)$ showing samples excluded based on their high molar $Al_2O_3/(Na_2O + K_2O + CaO)$ and samples that remain in the sample pool

Except for S-type granitic magmas, most magmas evolve from metaluminous compositions towards increasingly aluminous compositions, with many becoming weakly peraluminous (i.e. ASI >1.0) at SiO_2 concentrations >70 wt%. Caution is required at this stage since this screen would eliminate any S-type granitic rocks, which can show high ASI (often significantly >1.2) at SiO_2 contents much lower than 70 wt%. A series (suite) of fresh, geologically related granitic samples that show ASI >1.1 and typically also a negative correlation between SiO_2 and ASI would quite likely reflect S-type magmatism and should not be subjected to this screen. To date, no such rocks have been identified within either the Yilgarn or Pilbara Cratons, although they do form minor components of other Archean cratons.

1.5 SiO_2 vs $K_2O + Na_2O$

On a plot of SiO_2 wt% vs $K_2O + Na_2O$ wt% (Fig. 6), samples that plot below a line with a slope of $y = 0.125x - 4.625$ are excluded based on their low $K_2O + Na_2O$, which is interpreted to reflect losses of alkali elements during alteration.

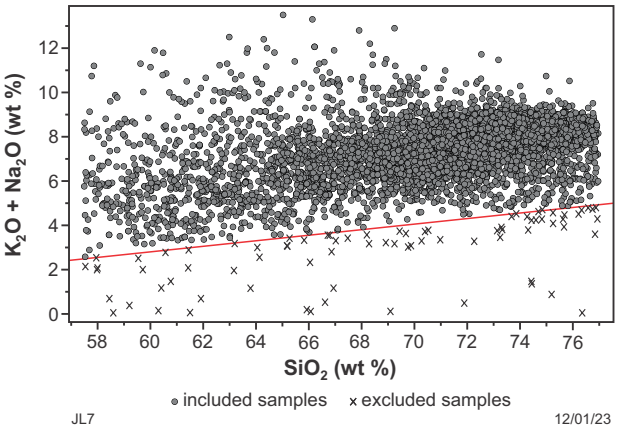

Figure 6. SiO_2 vs $K_2O + Na_2O$ showing samples excluded based on their low $K_2O + Na_2O$ and samples that remain in the sample pool

Consolidation of data screening calculations

All data screening steps have been consolidated into a single calculation that is provided in the MS Excel data file (Appendix 1) and in the calculation file for ioGAS (Appendix 3). If any sample meets one or more of the data screening criteria, then the 'Data Screening' column for that sample will output a value of '1' and the granite classification will be attributed as 'Unclassified'. If the data screening output value is '0', then the granite will be assessed by the following steps and attributed with a valid granite classification.

Step 2. Separate High-HFSE granite group from sample pool

Champion and Sheraton (1997) originally identified and distinguished the Archean High-HFSE granite group based on clear, evolved, tholeiitic characteristics typically including a relatively anhydrous mineralogy and strong enrichments in iron, HFSE, Y, REE (characteristically with flat and elevated mantle-normalized M-HREE patterns), Th, U and halogens. A significant mantle source component and a trend towards A-type compositions were suggested.

Samples that do not meet any of the data screening criteria are assessed by Steps 2.1–2.6.

2.1 SiO_2 vs Fe_2O_3T

On a plot of SiO_2 wt% vs Fe_2O_3T wt% (Fig. 7), samples that plot to the right of a line with a slope of $y = -0.4762x + 37.143$ (i.e. high Fe_2O_3T samples) are possible High-HFSE group samples and are assessed by Step 2.2. The remaining samples are returned into the sample pool to be assessed against diagnostic criteria for the High-Ca, Low-Ca and Mafic granite groups.

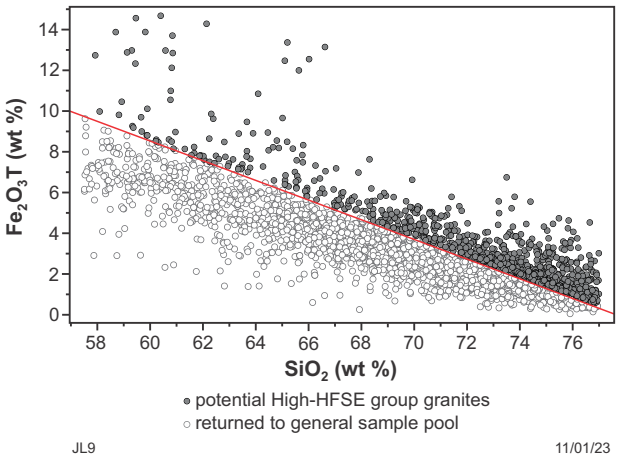

Figure 7. SiO_2 vs Fe_2O_3T showing samples that meet Step 2.1 criteria for High-HFSE group granites (high Fe_2O_3T) and samples that are returned to the sample pool

2.2 Yb vs Dy/Yb

Samples with Yb concentrations ≥1 ppm and Dy/Yb ratios ≥1 and ≤2.5 are possible High-HFSE group samples (Fig. 8) and are assessed by Step 2.3. The remaining samples are returned into the sample pool.

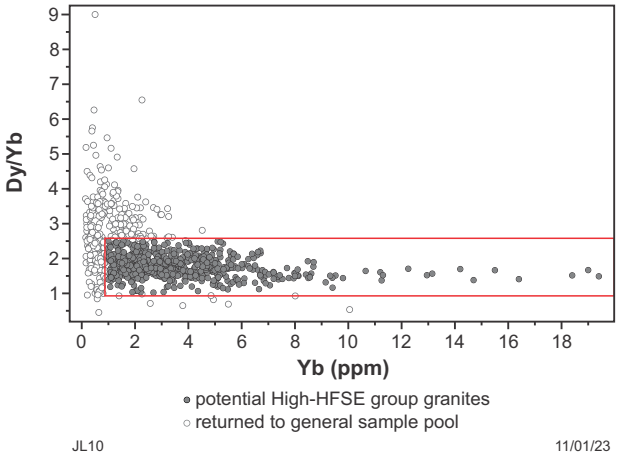

Figure 8. Yb vs Dy/Yb showing samples that meet Step 2.2 criteria for High-HFSE group granites (low Dy/Yb ratio at moderate–high Yb concentration) and samples that are returned to the sample pool

2.3 Sr/Sr* vs Rb/Y

Samples with Sr/Sr* [(Sr/21.1)/(sqrt((Pr/0.278)*(Nd/1.366)))] < 0.4 and Rb/Y <7 are included in High-HFSE group selection (Fig. 9) and are assessed by Step 2.4. The remaining samples are returned to the sample pool.

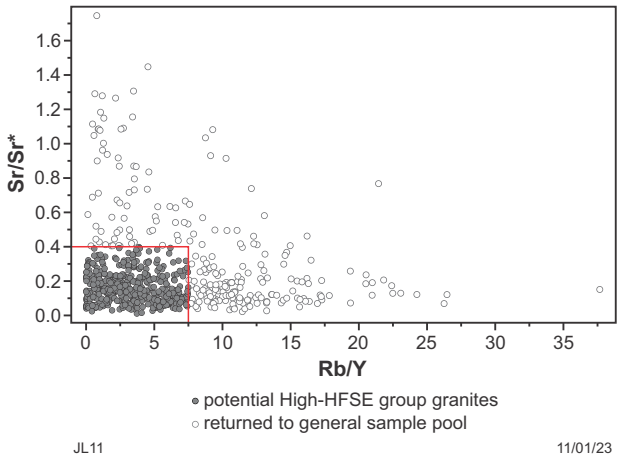

Figure 9. Rb/Y vs Sr/Sr* showing samples that meet Step 2.3 criteria for High-HFSE group granites (low Sr/Sr* and low Rb/Y) and samples that are returned to the sample pool

2.4 Th vs Al_2O_3

On a plot of Th ppm vs Al_2O_3 wt% (Fig. 10), samples that plot to the left of a line with a slope of $y = -0.07x + 16$ (i.e. low Th vs Al_2O_3 samples) are included in High-HFSE group selection and are assessed by Step 2.5. The remaining samples are returned to the sample pool.

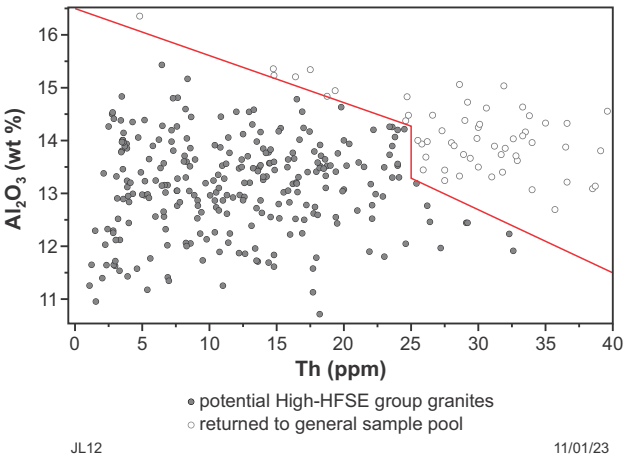

Figure 10. Th vs Al_2O_3 showing samples that meet Step 2.4 criteria for High-HFSE group granites (low Th vs Al_2O_3) and those that are returned to the sample pool

2.5 SiO_2 vs Mg-number

Samples containing ≤66 wt% SiO_2 with Mg-numbers ≥50 (Fig. 11) are returned to the sample pool. The remaining samples are included in the High-HFSE group selection and are assessed by Step 2.6.

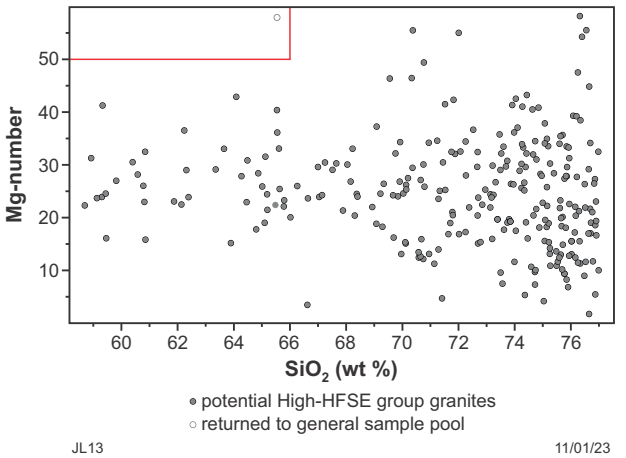

Figure 11. SiO_2 vs Mg-number showing samples that meet Step 2.5 criteria for High-HFSE group granites (low Mg-number vs SiO_2) and those that are returned to the sample pool

2.6 Al_2O_3 vs Pb

On a plot of Al_2O_3 wt% vs Pb ppm (Fig. 12), samples that plot to the left of a line with a slope of $y = 32x + 482$ *or* contain <10 ppm Pb at Al_2O_3 >14.8 wt% are assigned to the High-HFSE granite group while the remaining samples are returned to the sample pool.

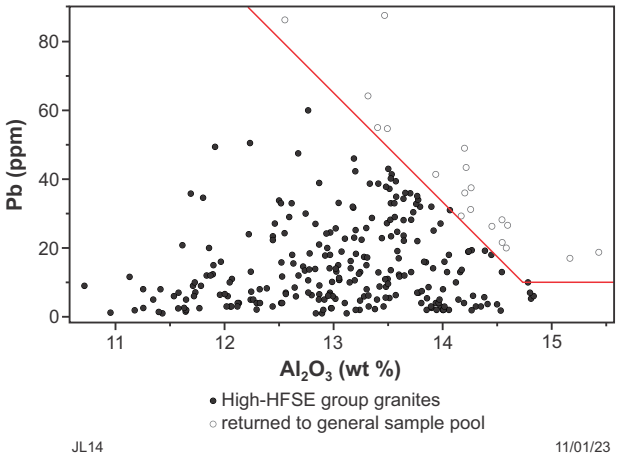

Figure 12. Al_2O_3 vs Pb showing samples that meet Step 2.6 criteria for High-HFSE group granites (low Al_2O_3 vs Pb) and those that are returned to the sample pool

Division of High-HFSE granite group into subgroups based on K_2O/Na_2O

Samples that meet the criteria for the High-HFSE granite group in Steps 2.1–2.6 and have K_2O/Na_2O ≥0.6 are classified as High-HFSE granite (K), whereas samples that have K_2O/Na_2O <0.6 are classified as High-HFSE granite (Na) (Fig. 13). Mantle normalized trace element patterns for High-HFSE (Na) and High-HFSE (K) granites in our dataset are shown in Figures 14 and 15 respectively.

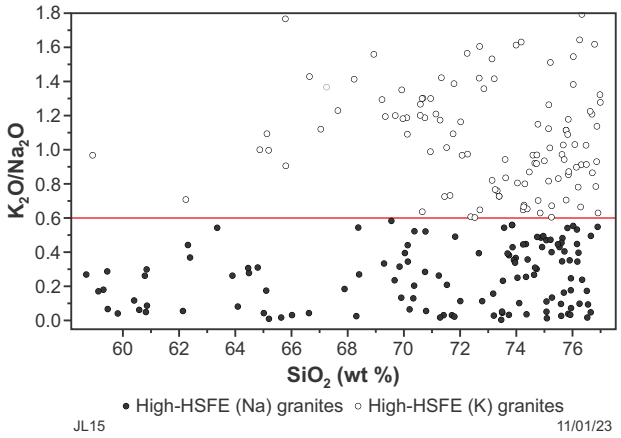

Figure 13. SiO_2 vs K_2O/Na_2O showing High-HFSE granite group samples divided based on K_2O/Na_2O into potassic 'High-HFSE (K)' granites and sodic 'High-HFSE (Na)' granites

Consolidation of High-HFSE granite calculations

All High-HFSE granite calculations have been consolidated into a single calculation that is provided in the MS Excel data file (Appendix 1) and in the calculation file for IoGAS (Appendix 3). If any sample meets all of the criteria above (i.e. Steps 2.1–2.6), then the cell in the 'High-HFSE granite group' column will have an output value of '1' and the granite classification will be attributed as either 'High-HFSE (Na) granite' or 'High-HFSE (K) granite' (depending on K_2O/Na_2O). If any sample fails to meet any one of the High-HFSE granite group criteria, then it is additionally assessed by Step 3.

Step 3. Separating Syenite group from the sample pool

Syenites are the only major Archean rock group of the Yilgarn Craton that fall entirely within the 'alkaline magma series' in terms of their position on a total alkalis vs SiO_2 (TAS) diagram (not shown), although none of the felsic groups comprise strictly 'alkaline rocks' in terms of having excess molecular Na + K over Al or Si (i.e. none is silica under-saturated or otherwise peralkaline – e.g. Shand, 1922).

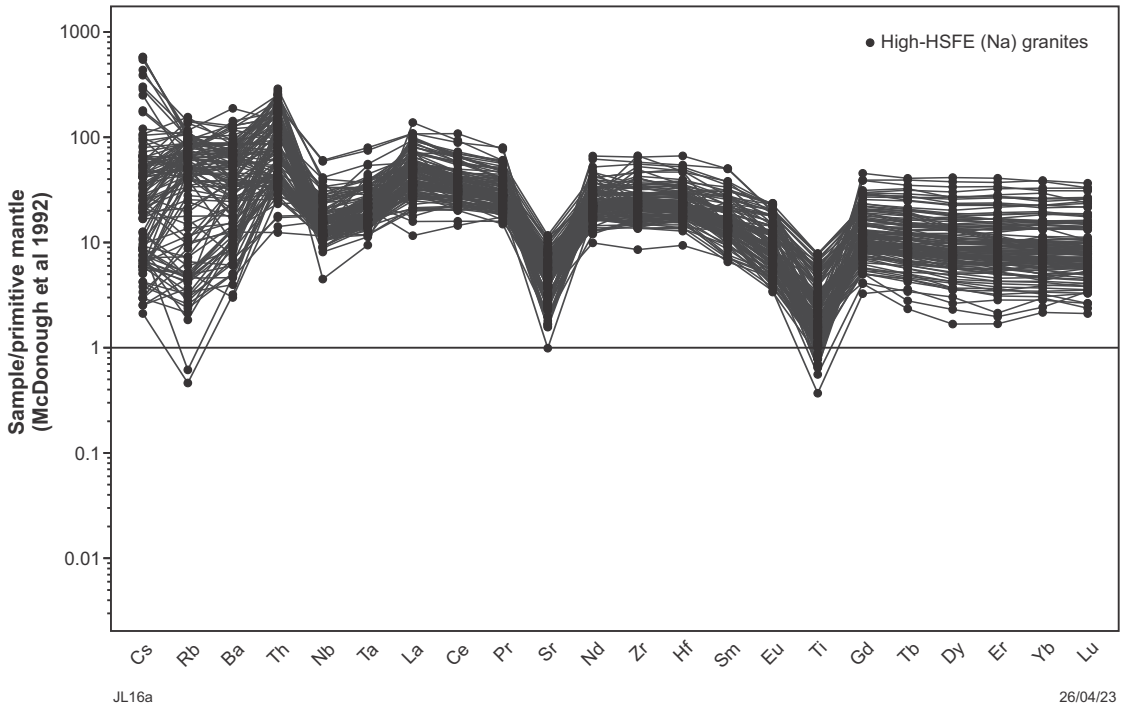

Figure 14. Primitive mantle (McDonough et al., 1992) normalized trace element patterns showing sodic High-HFSE (Na) granite samples

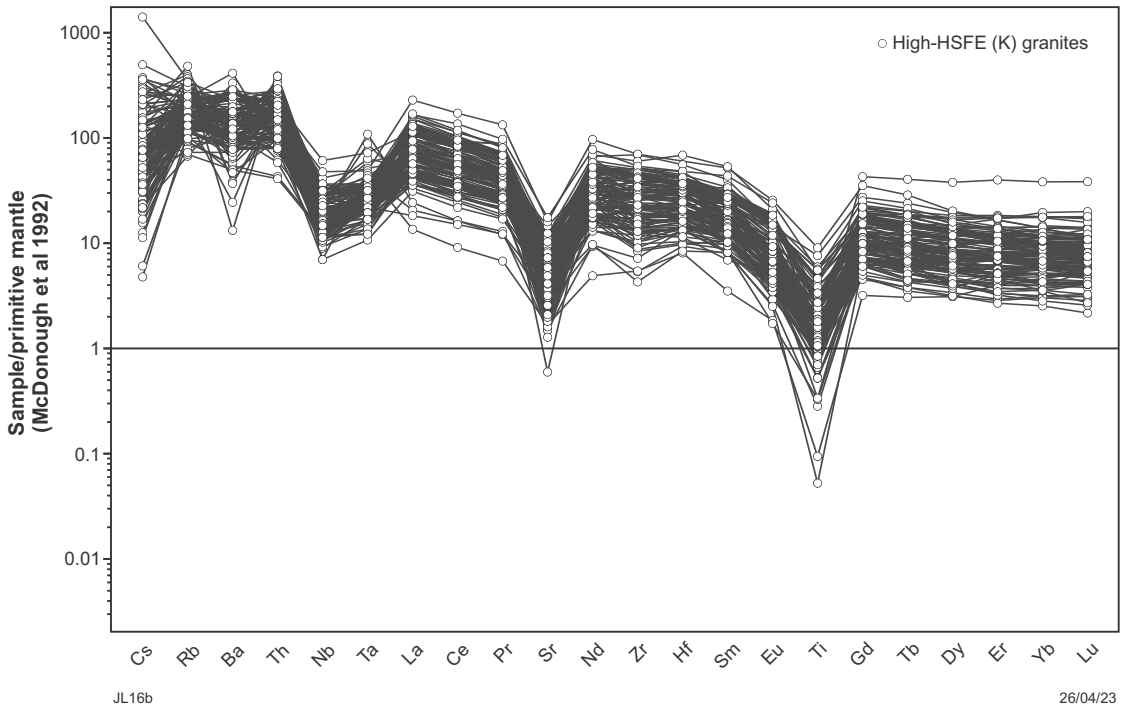

Figure 15. Primitive mantle (McDonough et al., 1992) normalized trace element patterns showing potassic High-HFSE (K) granite samples

Only samples that *do not* meet the consolidated data screening and High-HFSE granite group calculations are assessed by this step.

3.1 $K_2O + Na_2O$ vs K_2O/Na_2O

On a plot of $K_2O + Na_2O$ wt% vs K_2O/Na_2O (Fig. 16), samples that plot to the right of a line with slope of $y = 1.6667x - 13.333$ are possible Syenite group samples based on their high concentrations of alkali elements ($K_2O + Na_2O$) and are assessed by Step 3.2. The remaining samples are returned to the sample pool.

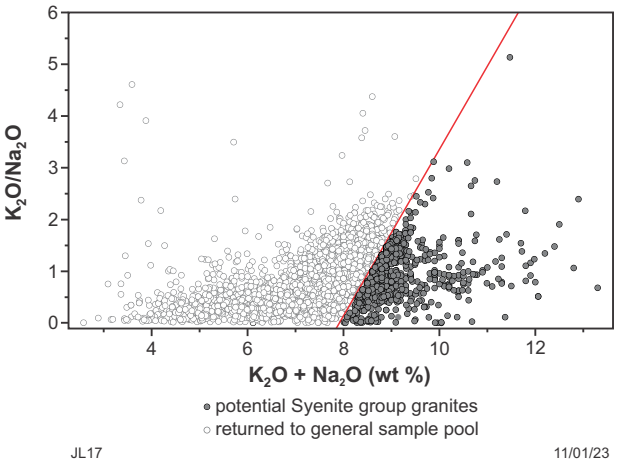

Figure 16. $K_2O + Na_2O$ vs K_2O/Na_2O showing samples that meet Step 3.1 criteria for the Syenite group (i.e. high $K_2O + Na_2O$ concentrations) and samples that are returned to the sample pool

3.2 $K_2O + Na_2O$ vs Rb/Sr

On a plot of $K_2O + Na_2O$ vs Rb/Sr (Fig. 17), samples that plot above a line with a slope of $y = 0.25x - 2$, where $K_2O + Na_2O \leq 10$ wt%, *or* have Rb/Sr <1.5, where $K_2O + Na_2O$ >10 wt%, are possible Syenite group samples based on their low Rb/Sr and are assessed by Step 3.3. The remaining samples are returned to the sample pool.

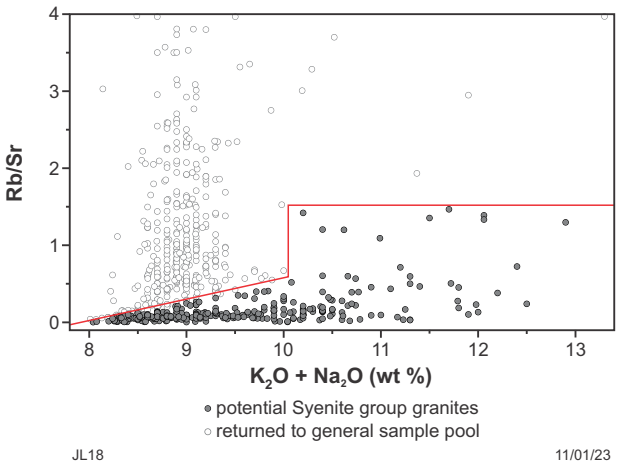

Figure 17. $K_2O + Na_2O$ vs Rb/Sr showing samples that meet Step 3.2 criteria for the Syenite group (low Rb/Sr vs $K_2O + Na_2O$) and samples that are returned to the sample pool

3.3 $K_2O + Na_2O$ concentration

Samples containing very high $K_2O + Na_2O$ (≥9.5 wt%) are assigned as Syenite group samples, while samples with moderate $K_2O + Na_2O$ (>8 wt% and ≤9.5 wt%) are possible Syenite group samples (black circles in Fig. 18) and are assessed by Step 3.4.

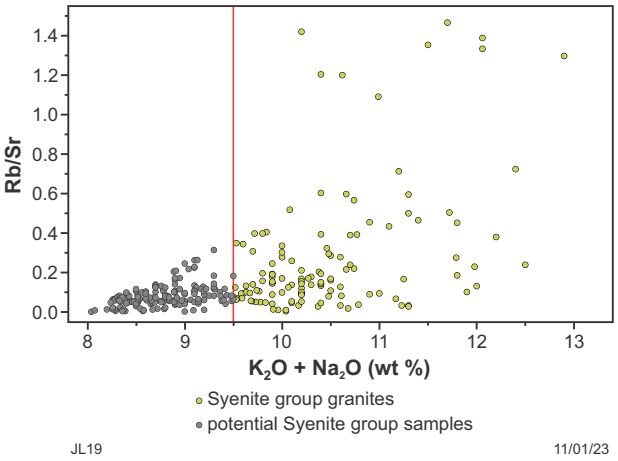

Figure 18. $K_2O + Na_2O$ vs Rb/Sr showing samples that meet Step 3.3 criteria for the Syenite group, i.e. very high $K_2O + Na_2O$ (≥9.5 wt%), that are assigned as Syenite group samples and samples with moderate $K_2O + Na_2O$ (>8 wt% and ≤9.5 wt%) that are possible Syenite group samples

3.4 SiO_2 vs Rb

On a plot of SiO_2 wt% vs Rb ppm (Fig. 19), samples that plot to the left of a line with a slope of $y = 62.5x - 4375$ are possible Syenite group samples based on their lower SiO_2 content. The remaining samples are returned to the sample pool.

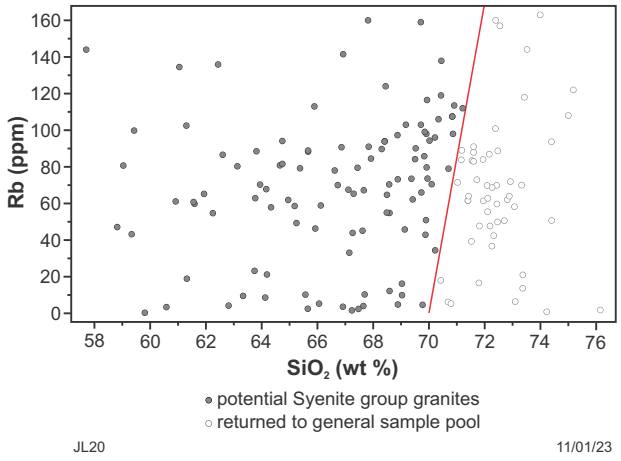

Figure 19. SiO_2 vs Rb showing samples that meet Step 3.4 criteria for the Syenite group and those that are returned to the sample pool

3.5 $K_2O + Na_2O$ vs Mg-number

On a plot of $K_2O + Na_2O$ wt% vs Mg-number (Fig. 20), samples containing ≥8.5 wt% $K_2O + Na_2O$ that plot to the right of a line with a slope of $y = 12x - 45$ are possible Syenite group samples based on their higher $K_2O + Na_2O$ vs Mg-number. The remaining samples will include Sanukitoids, Sanukitoid-like rocks and some Diorites and are returned to the sample pool.

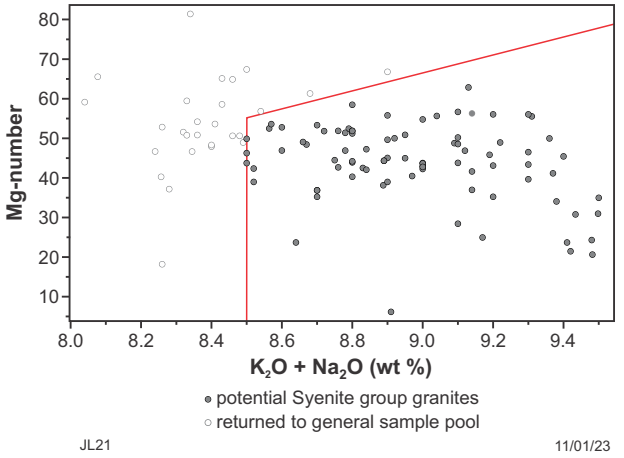

Figure 20. $K_2O + Na_2O$ vs Mg-number showing samples that meet Step 3.5 criteria for the Syenite group and those that are returned to the sample pool

3.6 Molar $Al_2O_3/(Na_2O + K_2O + CaO)$ vs molar $CaO/(Na_2O + K_2O + CaO)$

On a plot of ASI (i.e. molar $Al_2O_3/(Na_2O + K_2O + CaO)$) vs molar $CaO/(Na_2O + K_2O + CaO)$ (Fig. 21), samples that plot to the left of a line with a slope of $y = -0.75x + 0.925$ are classified as Syenite group samples. Samples that plot to the right of the line are considered to have more calc-alkaline, rather than alkaline affinities, and are returned to the sample pool.

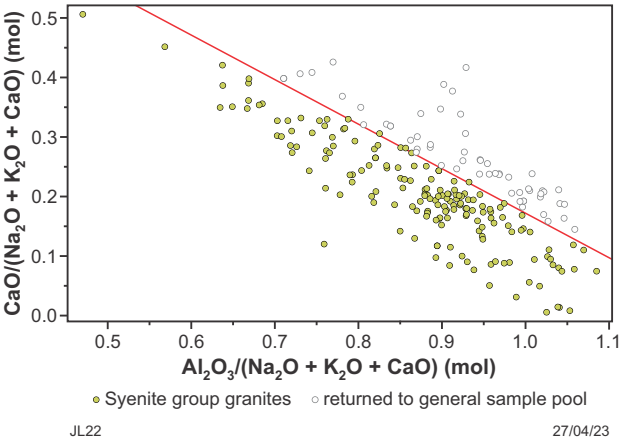

Figure 21. Molar $Al_2O_3/(Na_2O + K_2O + CaO)$ vs molar $CaO/(Na_2O + K_2O + CaO)$ showing samples that meet Step 3.6 criteria for the Syenite group and those that are returned to the sample pool

Division of Syenite group into subgroups based on K_2O/Na_2O

Samples that meet the criteria for the Syenite group in Steps 3.1–3.6 and have K_2O/Na_2O ≥0.6 are classified as Syenite (K), whereas samples that have K_2O/Na_2O <0.6 are classified as Syenite (Na) (Fig. 22). Mantle normalized trace element patterns for Syenite (Na) and Syenite (K) are shown in Figures 23 and 24 respectively.

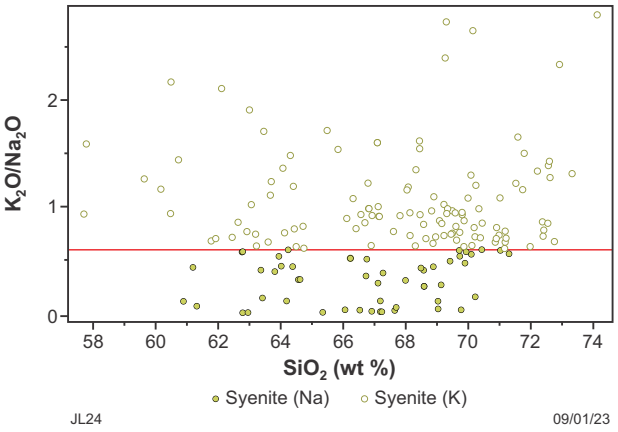

Figure 22. SiO_2 vs K_2O/Na_2O showing Syenite group samples divided based on K_2O/Na_2O into potassic 'Syenite (K)' and sodic 'Syenite (Na)'

Consolidation of Syenite calculations

All Syenite calculations have been consolidated into a single calculation that is provided in the MS Excel data file (Appendix 1) and the calculation file for ioGAS (Appendix 3). If any sample meets all of the criteria above (i.e. Steps 3.1– 3.6), then the cell in the 'Syenite group' column will have an output of '1' and the granite classification will be attributed as either 'Syenite (Na)' or 'Syenite (K)' (depending on K_2O/Na_2O). If any sample fails to meet any one of the Syenite group criteria, then it is additionally assessed by Step 4.

Step 4. First pass separation of remaining samples into High-Ca, Low-Ca and Mafic granite groups

Only samples that do not meet the consolidated data screening, High-HFSE granite group and Syenite group calculations are assessed against Step 4.

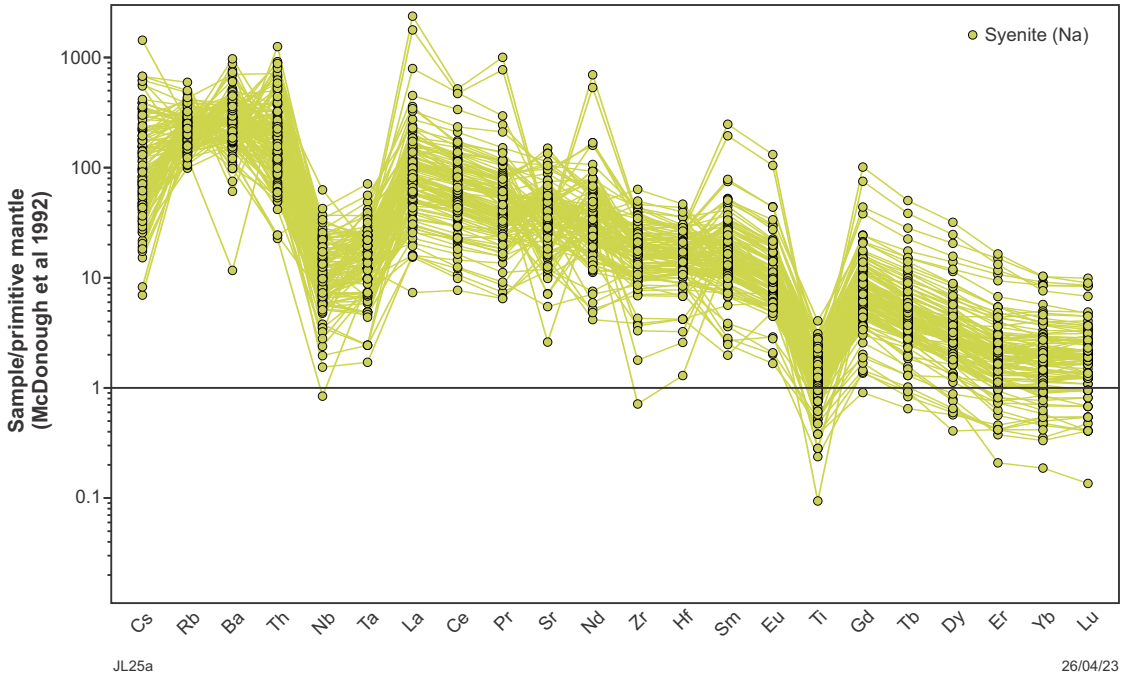

Figure 23. Primitive mantle (McDonough et al., 1992) normalized trace element patterns showing sodic Syenite (Na) samples

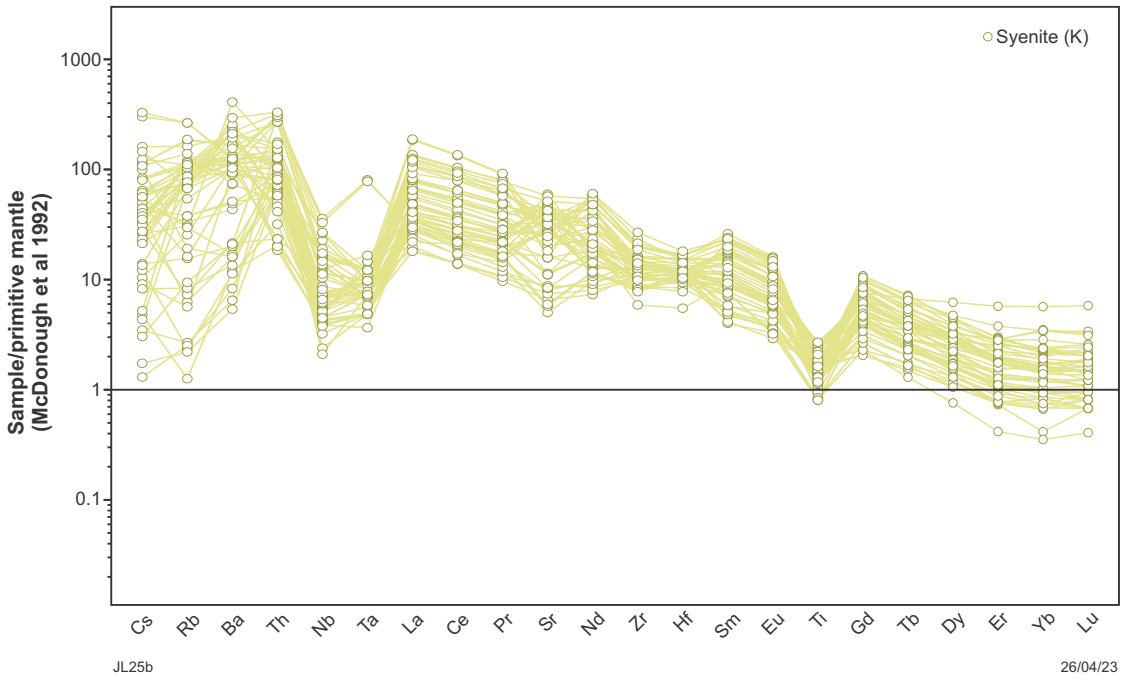

Figure 24. Primitive mantle (McDonough et al., 1992) normalized trace element patterns showing potassic Syenite (K) samples

4.1 SiO_2 vs Mg-number

On a plot of SiO_2 wt% vs Mg-number (Fig. 25), samples that contain <67 wt% SiO_2 and have Mg-numbers ≥40, *or* samples that contain ≥67 wt% SiO_2 and plot above a line with a slope of $y = 1.875x - 85.625$ are tentatively classified as Mafic granite group samples (later reassessed in Steps 5.1, 5.2 and 5.3 to determine if any are instead High-Ca granites). The remaining samples are additionally assessed in Step 4.2.

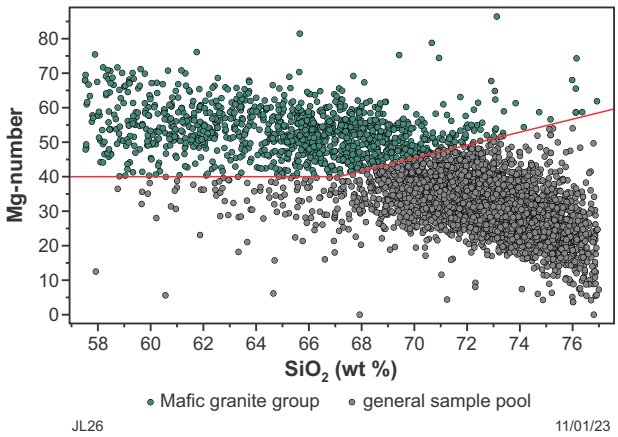

Figure 25. SiO_2 vs Mg-number showing samples that are classified in Step 4.1 as Mafic granite samples and samples that require further assessment before assigning into Mafic, Low-Ca and High-Ca granite groups

4.2 K_2O vs Ce

On a plot of K_2O wt% vs Ce ppm (Fig. 26), samples that plot to the left of a line with a slope of $y = -66.667x + 300$ are tentatively classified as High-Ca granite group samples (later reassessed in Step 5.1 to determine if any are rather Mafic granites). Samples that plot to the right of a line with a slope of $y = -87.5x + 525$ and all samples with >5.5 wt% K_2O are tentatively classified as Low-Ca granite group samples (later reassessed in Step 8 to determine if any are rather Mafic granites). Samples that plot between those two lines could be High-Ca granites, Low-Ca granites or Mafic granites and remain in the sample pool to be assessed in Step 4.3.

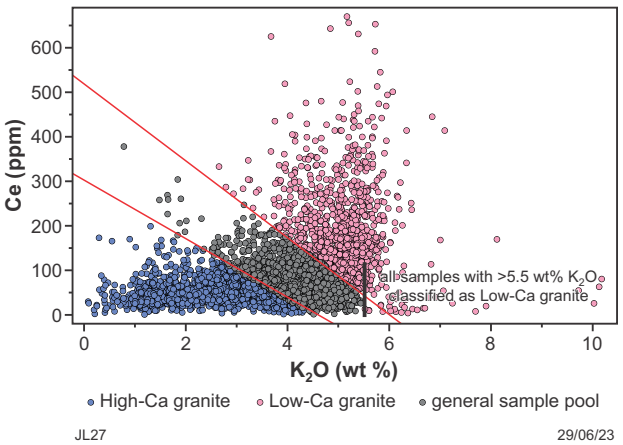

Figure 26. K_2O vs Ce showing samples that are classified in Step 4.2 as High-Ca or Low-Ca granite group samples and samples remain in the sample pool to be assessed in Step 4.3

4.3 Na_2O vs K_2O

On a plot of Na_2O wt% vs K_2O wt% (Fig. 27), samples that plot to the right of a line with a slope of $y = -0.3333x + 6.0833$ are tentatively classified as Low-Ca granite group samples. The remaining samples remain in the sample pool to be assessed in Step 4.4.

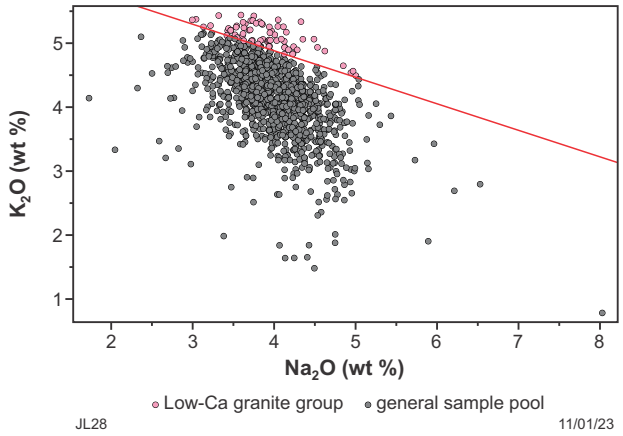

Figure 27. Na_2O vs K_2O showing samples that are classified in Step 4.3 as Low-Ca granite group samples and samples that remain in the sample pool

4.4 Yttrium concentration

Samples that contain greater than 60 ppm Y are tentatively classified as Low-Ca granite group (see Y vs SiO_2 plotted in Fig. 28). The remaining samples remain in the sample pool to be assessed in Step 4.5.

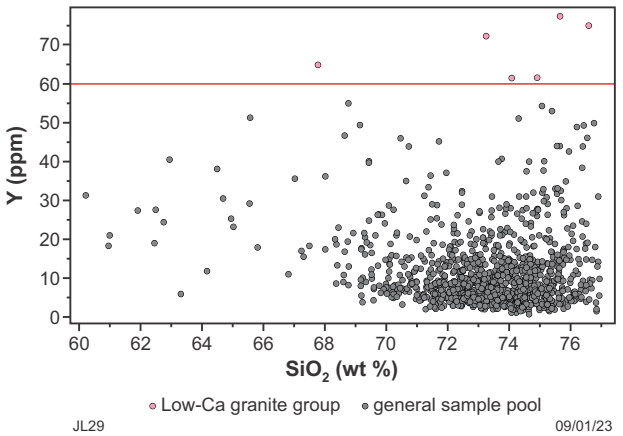

Figure 28. SiO_2 vs Y showing samples that are classified in Step 4.4 as Low-Ca granite group samples and samples that remain in the sample pool

4.5 Ce + (5*Th) + Zr + (10*Y) vs Sr

Samples that contain >300 ppm Sr and have (Ce ppm + (5*Th ppm) + Zr ppm + (10*Y ppm)) <400 are tentatively classified as High-Ca granite group (Fig. 29). Samples that contain <400 ppm Sr and have (Ce ppm + (5*Th ppm) + Zr ppm + (10*Y ppm)) >700 are tentatively classified as Low-Ca granite group (Fig. 31). The remaining samples remain in the sample pool to be assessed in Step 4.6.

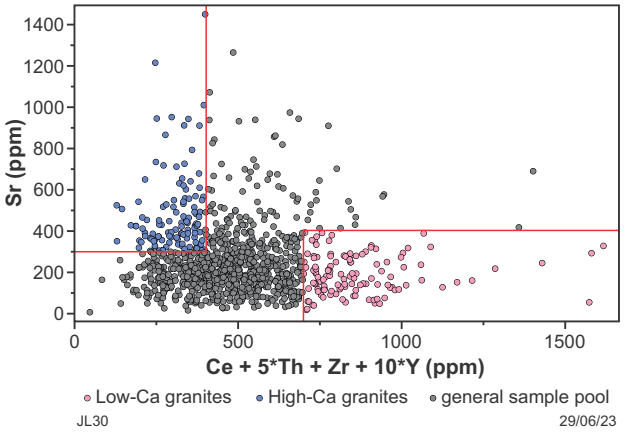

Figure 29. Ce + (5*Th) + Zr + (10*Y) vs Sr showing samples that are classified in Step 4.5 as High-Ca or Low-Ca granite group and samples that remain in the sample pool

4.6 CaO vs Ce

On a plot of CaO wt% vs Ce ppm (Fig. 30), samples that plot to the right of a line with a slope of $y = 226.67x - 386.67$ and contain ≤180 ppm Ce are tentatively classified as High-Ca granite group. Samples that plot to the left of a line with a slope of $y = 100x - 50$ *or* contain >180 ppm Ce are tentatively classified as Low-Ca granite group. The remaining samples remain in the sample pool to be assessed in Step 4.7.

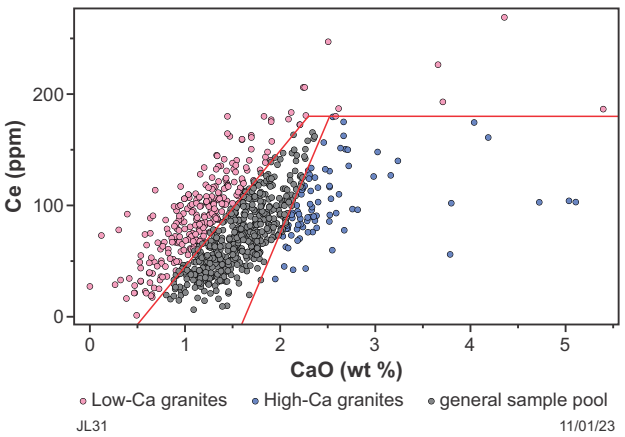

Figure 30. CaO vs Ce showing samples that are classified in Step 4.6 as High-Ca or Low-Ca granite group samples and samples that remain in the sample pool

4.7 SiO_2 vs Al_2O_3

On a plot of SiO_2 wt% vs Al_2O_3 wt% (Fig. 31), samples that plot to the right of a line with a slope of $y = -0.2778x + 35$ are tentatively classified as High-Ca granite group. The remaining samples remain in the sample pool and are additionally assessed in Step 4.8.

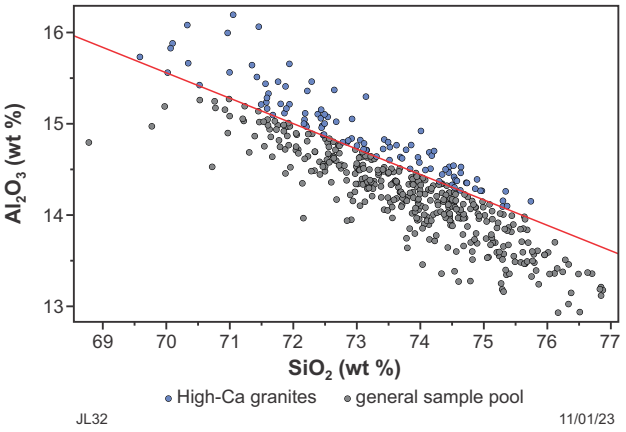

Figure 31. SiO_2 vs Al_2O_3 showing samples that are classified in Step 4.7 as High-Ca granites and samples that remain in the sample pool

4.8 SiO_2 vs Fe_2O_3T

On a plot of SiO_2 wt% vs Fe_2O_3T wt% (Fig. 32), samples that plot to the left a line with a slope of $y = -0.3889x + 30.056$ *or* to the left of a line with a slope of $y = -0.6111x + 45.944$ are tentatively classified as High-Ca granite group. The remaining samples remain in the sample pool and are additionally assessed in Step 4.9.

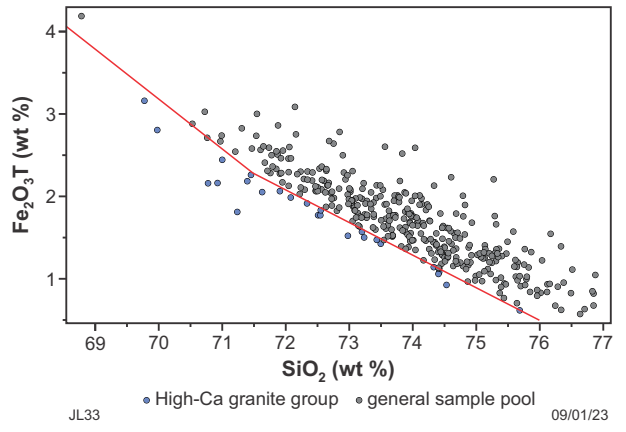

Figure 32. SiO_2 vs Fe_2O_3T showing samples that are classified in Step 4.8 as High-Ca granite group samples and samples that remain in the sample pool

4.9 Sr/Sr*

Samples that have Sr/Sr* ≥1 are tentatively classified as High-Ca granite group, whereas the remaining samples are tentatively classified as Low-Ca granite group (Fig. 33). At this stage in the classification process, all samples that passed beyond the data screening process (Step 1) should have tentatively been assigned to one of the five granite groups.

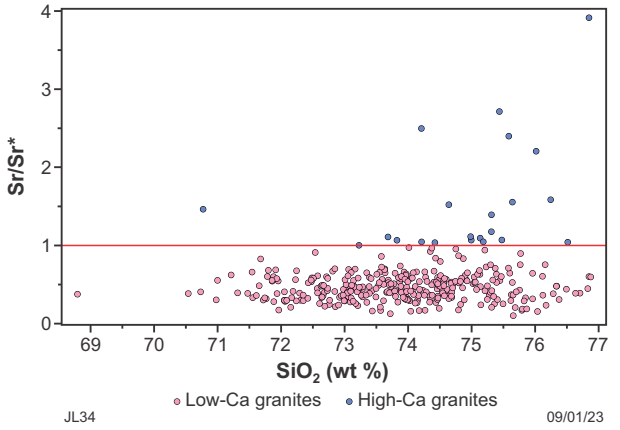

Figure 33. SiO_2 vs Sr/Sr* showing samples that are classified in Step 4.9 as High-Ca or Low-Ca granite group

Step 5. Redistributing samples between High-Ca granite and Mafic granite groups

5.1 Mg-number vs Sr

On a plot of Mg-number vs Sr ppm (Fig. 34), samples that are tentatively classified as High-Ca granites at the completion of Step 4 and plot to the right of a line with a slope of $y = -200x + 9000$ are reclassified as Mafic granites.

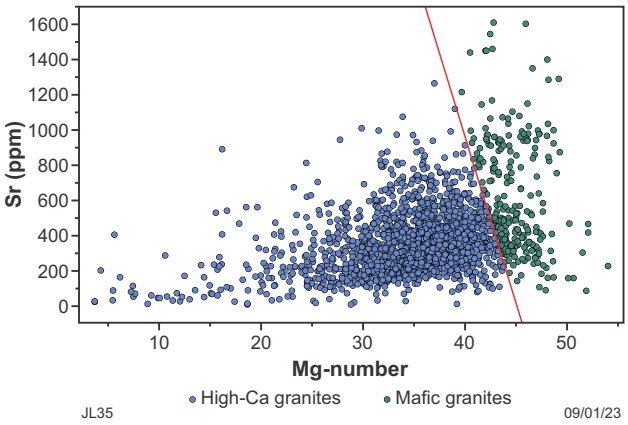

Figure 34. Mg-number vs Sr showing samples that are reclassified in Step 5.1 from the High-Ca granite group to the Mafic granite group

5.2 SiO_2 vs Zr

On a plot of SiO_2 wt% vs Zr ppm (Fig. 35), samples that are tentatively classified as Mafic granite group at the completion of Step 5.1 and plot to the right of a line with a slope of $y = -25x + 1950$ are reclassified as High-Ca granites.

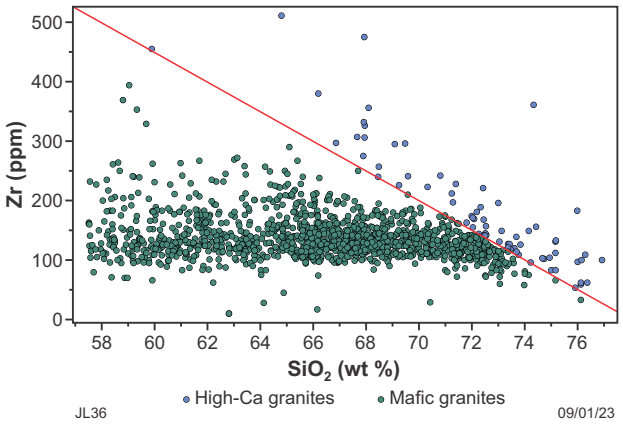

Figure 35. SiO_2 vs Zr showing samples that are reclassified in Step 5.2 from the Mafic granite group to High-Ca granite group

5.3 SiO_2 vs Zr/Zr*

On a plot of SiO_2 vs Zr/Zr* (Fig. 36), samples that are classified as Mafic granite group at the completion of Step 5.2 are reclassified as High-Ca granites if they contain >68 wt% SiO_2 and have Zr/Zr* ratios >1.7. Furthermore, samples that plot to the right of a line with a slope of $y = 0.0923x - 6.1308$ are reclassified as 'Unclassified' due to their very low Zr/Zr* ratios at high SiO_2 concentration.

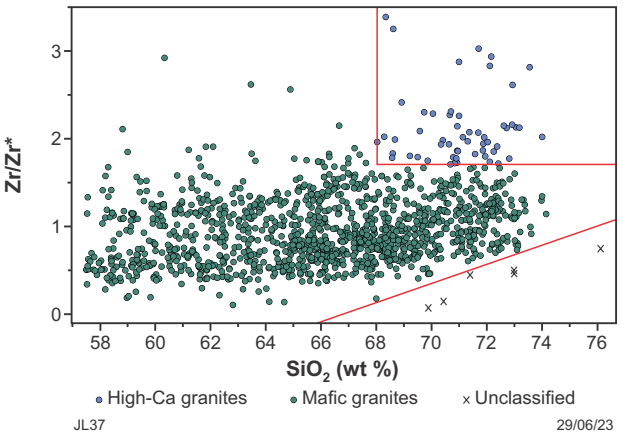

Figure 36. SiO_2 vs Zr/Zr* showing samples that are reclassified in Step 5.3 from Mafic granite group to High-Ca granite group or to 'Unclassified'

5.4 Rb/Y vs K_2O

Samples that are classified as Mafic granite group are reassessed on a plot of Rb/Y vs K_2O wt% (Fig. 37). Samples that plot to the right of a line with a slope of $y = 0.225x - 0.625$ are reclassified as High-Ca granite group.

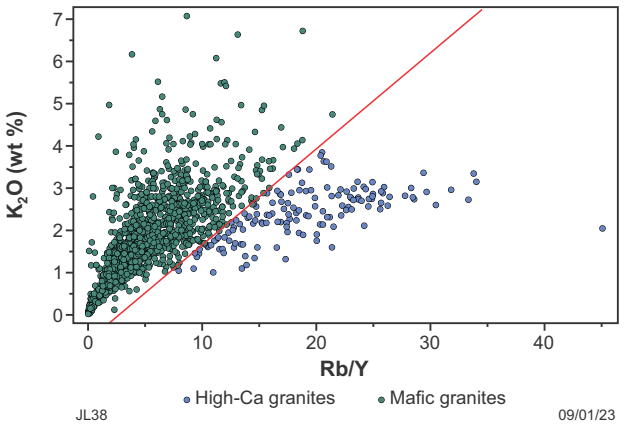

Figure 37. K_2O vs Rb/Y showing samples that are reclassified from Mafic granite group to High-Ca granite group

5.5 SiO_2 concentration

Samples that are classified as High-Ca granite group are reassessed based on their SiO_2 concentration with samples containing <67 wt% SiO_2 being reclassified to the Mafic granite group (SiO_2 plotted against Zr, as an example, in Fig. 38).

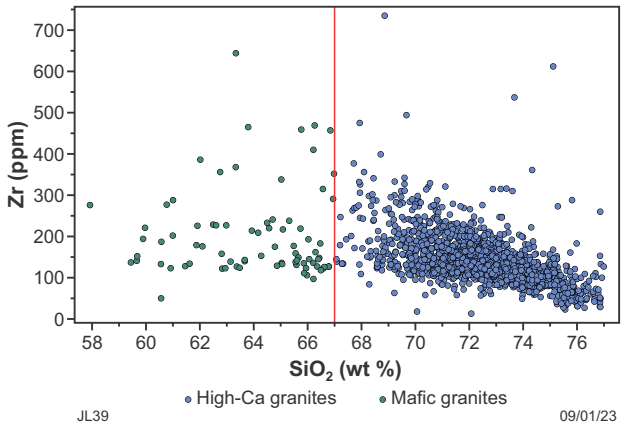

Figure 38. SiO_2 vs Zr showing samples that are reclassified from the High-Ca granite group to the Mafic granite group

Step 6. Division of High-Ca granite group into subgroups

Champion and Cassidy (2002) recognised a number of subgroups within the High-Ca granites: primarily in the LILE contents: 1) a high Na_2O, lower-LILE subgroup typical of Archean TTGs in general, and 2) less common, higher-LILE (lower Na_2O, Na/K) subgroups with characteristics becoming intermediate between High-Ca and Low-Ca compositions. They also recognised, within these two endmembers, as additional subgroups characterised by variations in Sr, HREE, Sr/Y, LREE/HREE–proxies reflecting variations in source compositions and melting conditions as greatly expanded on by Smithies et al. (2018). We have expanded and more formally characterised these subgroups.

6.1 Division based on K_2O/Na_2O

High-Ca granites are divided into 'very sodic' (Na+; K_2O/Na_2O 0–0.6) 'sodic' (Na; K_2O/Na_2O >0.6–1.0) and 'potassic' (K; K_2O/Na_2O >1.0) subgroups (Fig. 39), reflecting the amount of reworked crustal material contributing K to otherwise K-poor 'basaltic' bulk source compositions and/or reflecting decreasing degrees of partial melting.

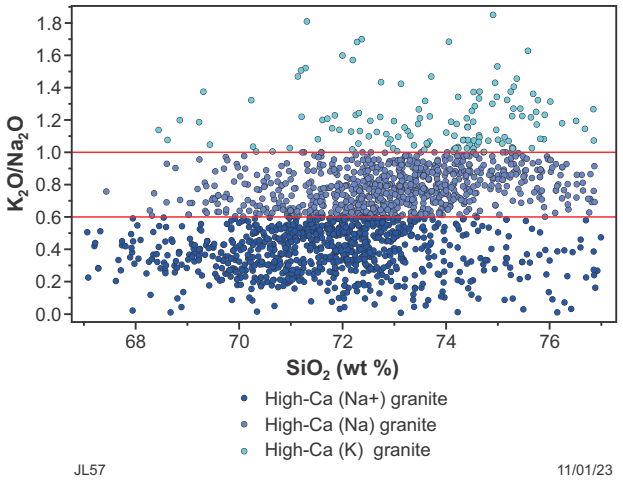

Figure 39. SiO_2 vs K_2O/Na_2O showing High-Ca granite group samples subdivided into very sodic (Na+), sodic (Na) and potassic (K)

6.2 Division based on Sr/Y

High-Ca granite group samples are also subdivided into high- and low-Sr/Y subgroups, reflecting enriched and/or deep (i.e. >40 km) sources (Sr/Y ≥40) or unenriched and/or shallow (<40 km) sources (Sr/Y <40), respectively (Fig. 40). Samples with Sr/Y ≥40 are classified as high-Sr/Y, whereas samples with Sr/Y <40 are classified as low-Sr/Y.

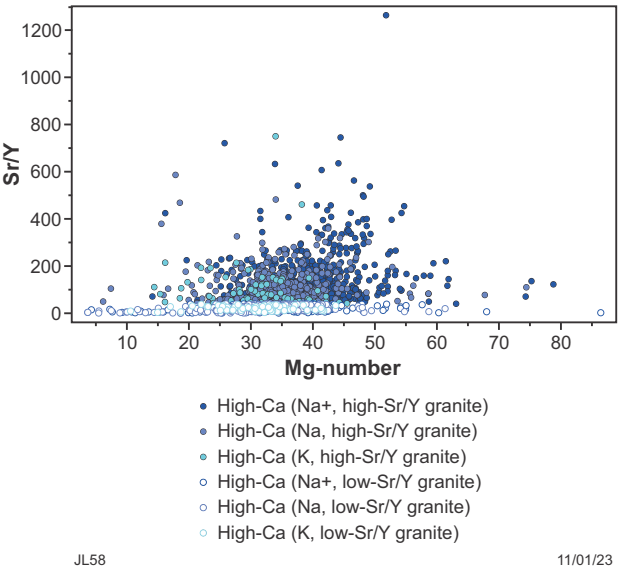

Figure 40. Sr/Y vs Mg-number showing High-Ca granite group samples subdivided into high Sr/Y and low-Sr/Y samples

Consolidation of High-Ca granite calculations

All High-Ca granite group calculations have been consolidated into a single calculation that is provided in the MS Excel data file (Appendix 1) and the calculation file for ioGAS (Appendix 3). If any sample meets all of the criteria for the High-Ca granite group (i.e. Steps 4.1–5.5), then the cell in the 'High-Ca granite group' column will output a value of '1' and the granite classification will be attributed as either 'High-Ca (Na+, high-Sr/Y) granite', 'High-Ca (Na, high-Sr/Y) granite', 'High-Ca (K, high-Sr/Y) granite', 'High-Ca (Na+, low-Sr/Y) granite', 'High-Ca (Na, low-Sr/Y) granite' or 'High-Ca (K, low-Sr/Y) granite' (depending on K_2O/Na_2O and Sr/Y). Mantle normalized trace element patterns for High-Ca granite subgroups in our dataset are shown in Figures 41–46.

Step 7. Division of Low-Ca granite group into subgroups

Low-Ca granites – ranging to higher SiO_2, K_2O and incompatible trace element concentrations than most High-Ca granites – reflect re-melting of a bulk source that on average is more evolved and drier than the source for High-Ca granites, and typically at higher temperatures. Champion and Cassidy (2002) subdivided the Low-Ca granites into subgroups (their 'clans') based largely on degree of enrichment of the LILE (and less so HFSE). They suggested these subgroups most likely represented changes in the degree of partial melt of a broadly similar source and/or variations in the source composition (including the possible involvement of High-Ca source rocks). Smithies et al (2021) identified a Ti- and P-rich subclass of Low-Ca granites, locally including orthopyroxene-bearing examples (i.e. charnockites) reflecting higher temperature crustal melting of a drier and/or more refractory source. Samples with these characteristics meet the criteria for all three of Steps 7.1, 7.2 and 7.3 and are divided from the Low-Ca granite group as 'Low-Ca (high-Ti) granite'. Samples that do not meet the criteria in any one of the Steps 7.1 – 7.3 remain classified into the Low-Ca granite subgroup.

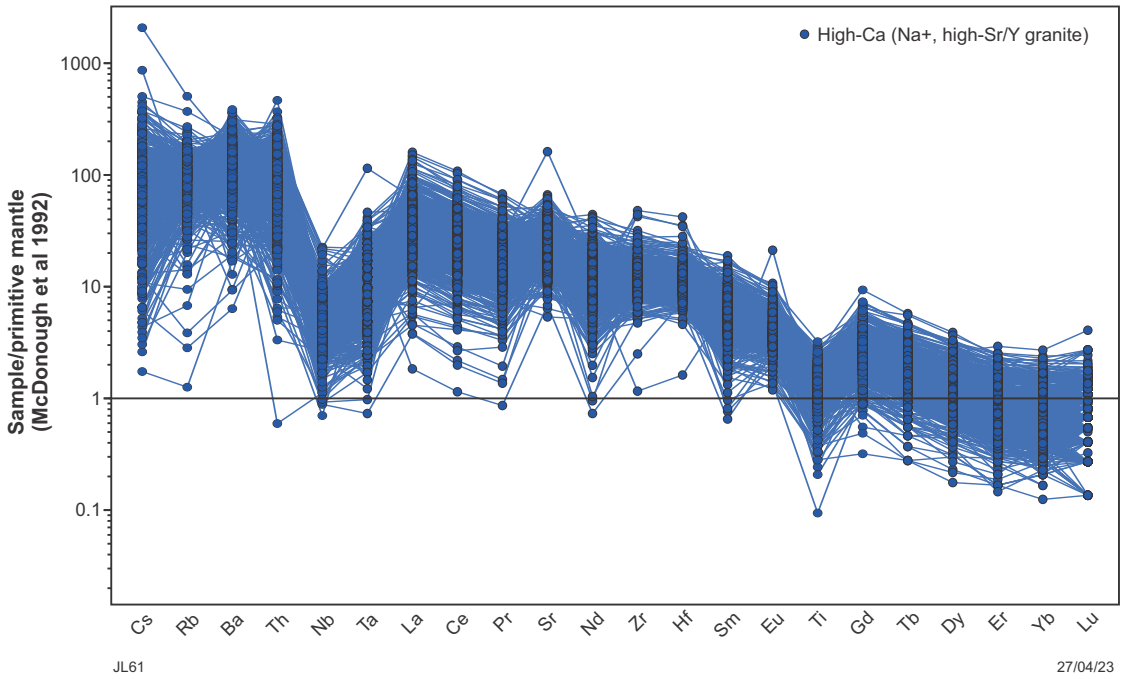

Figure 41. Primitive mantle (McDonough et al., 1992) normalized trace element patterns showing High-Ca (Na+, high-Sr/Y) granite samples

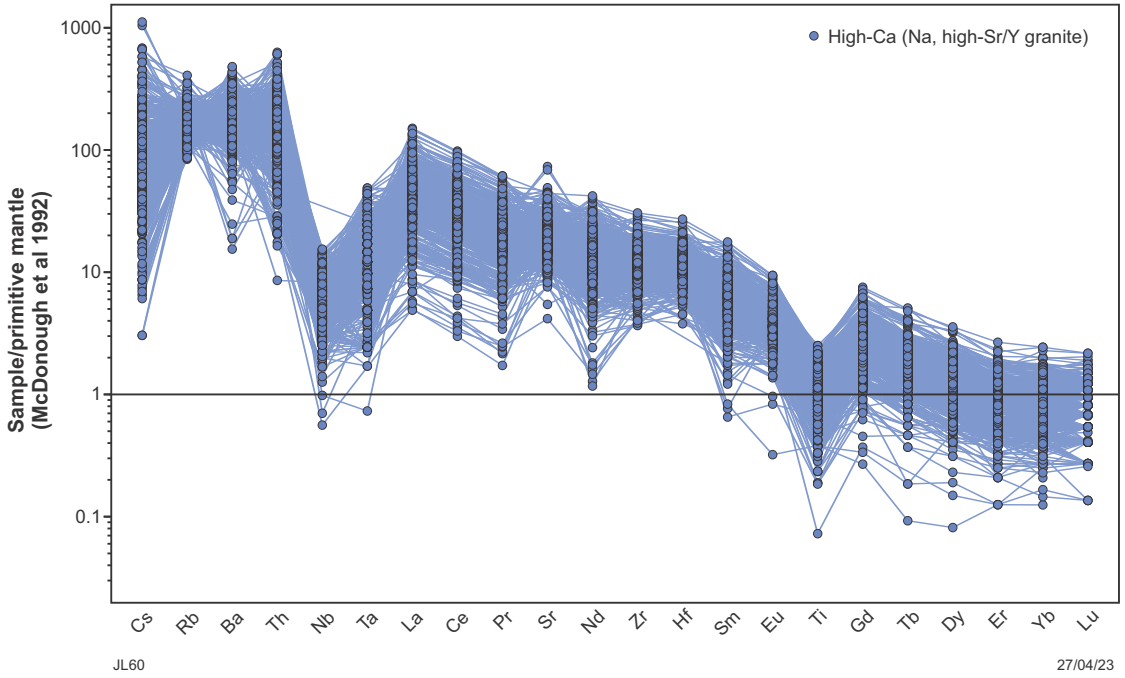

Figure 42. Primitive mantle (McDonough et al., 1992) normalized trace element patterns showing High-Ca (Na, high-Sr/Y) granite samples

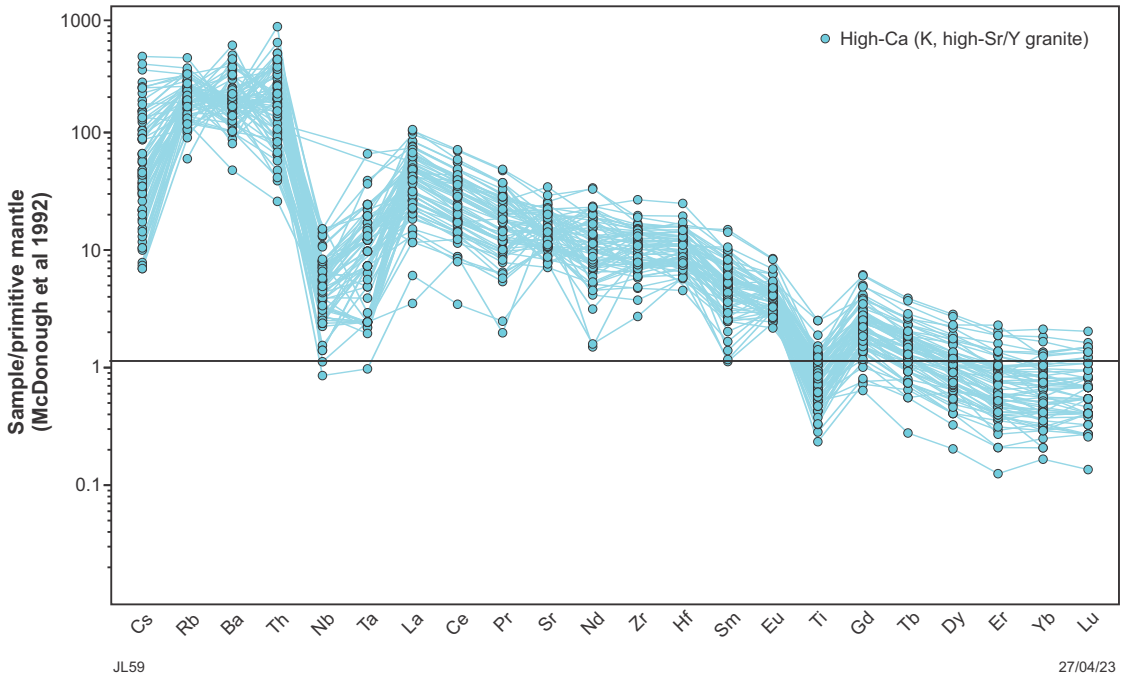

Figure 43. Primitive mantle (McDonough et al., 1992) normalized trace element patterns showing High-Ca (K, high-Sr/Y) granite samples

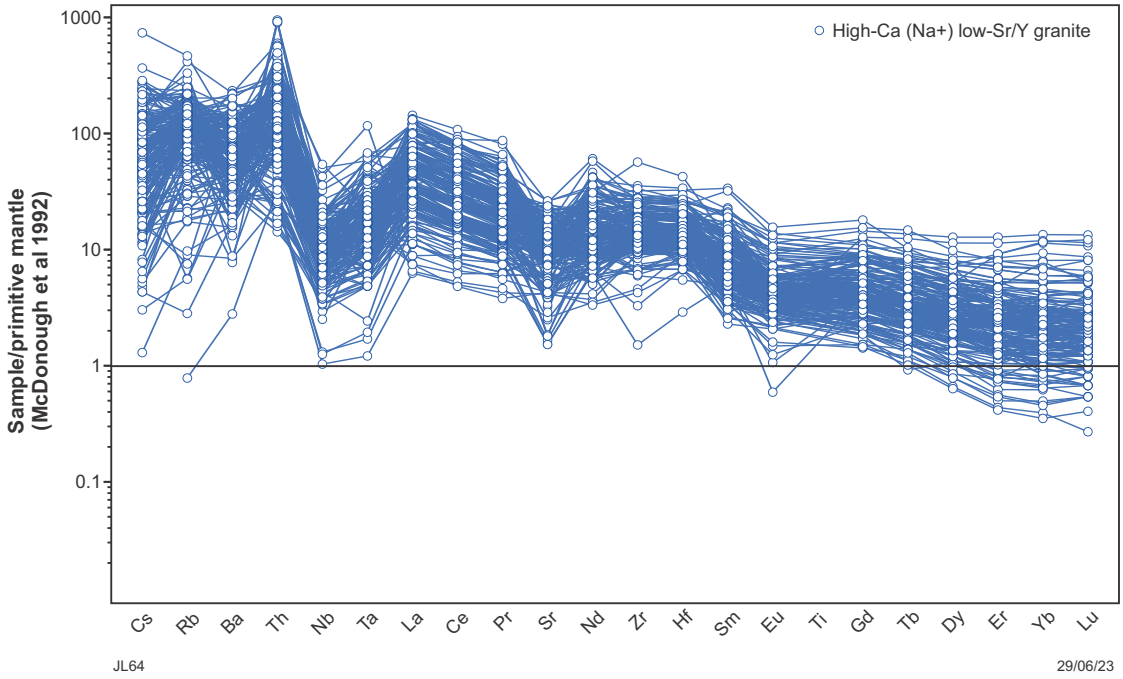

Figure 44. Primitive mantle (McDonough et al., 1992) normalized trace element patterns showing High-Ca (Na+, low-Sr/Y) granite samples

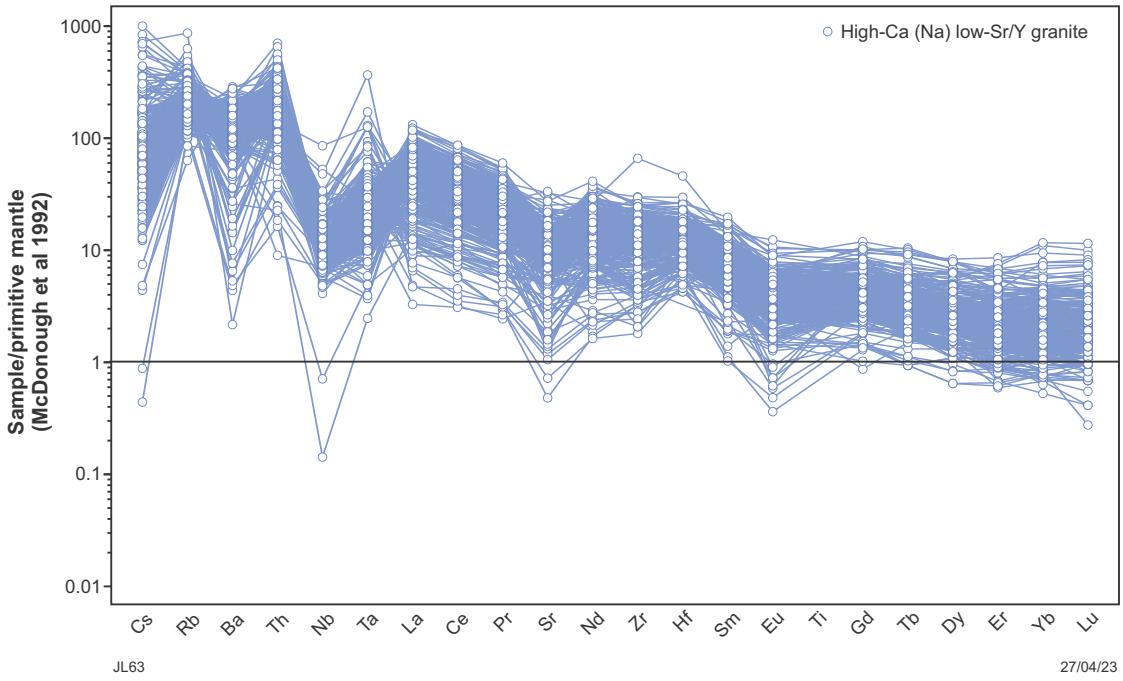

Figure 45. Primitive mantle (McDonough et al., 1992) normalized trace element patterns showing High-Ca (Na, low-Sr/Y) granite samples

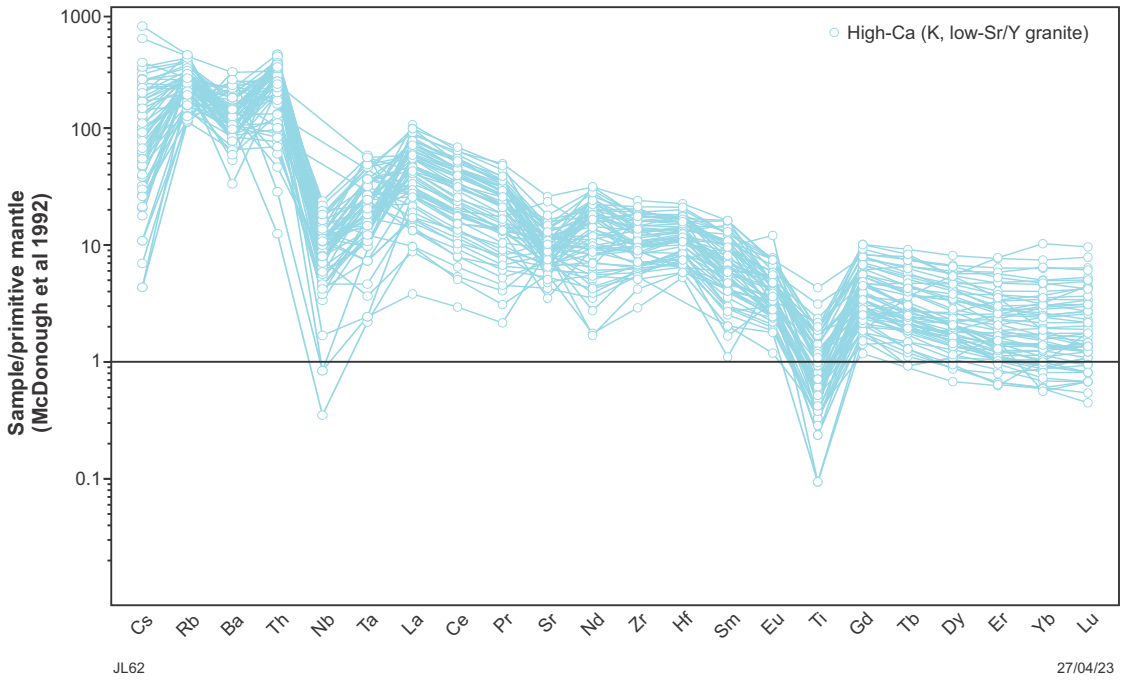

Figure 46. Primitive mantle (McDonough et al., 1992) normalized trace element patterns showing High-Ca (K, low-Sr/Y) granite samples

7.1 SiO_2 vs TiO_2

On a plot of SiO_2 wt% vs TiO_2 wt% (Fig. 47), samples that plot above a line with a slope of $y = -0.044x + 3.5$ meet one of the three criteria for Low-Ca (high-Ti) granite samples. The remaining samples are classified into the Low-Ca granite subgroup.

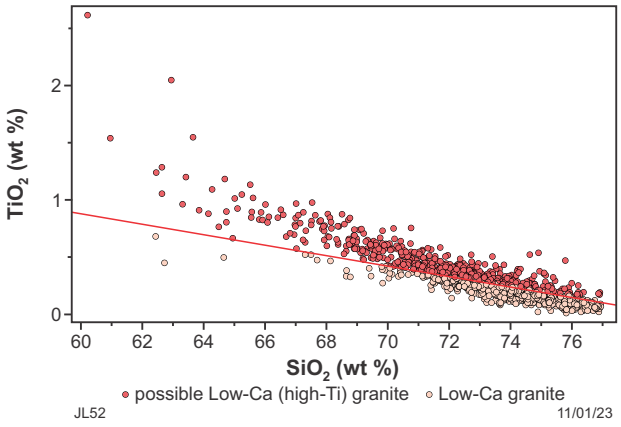

Figure 47. SiO_2 vs TiO_2 showing samples that classify by the Step 7.1 criteria as possible Low-Ca (high-Ti) granite samples and those that remain as Low-Ca granite

7.2 SiO_2 vs Al_2O_3

Samples that meet the criteria of Step 7.1 are additionally assessed in Step 7.2. On a plot of SiO_2 wt% vs Al_2O_3 wt% (Fig. 48), samples that plot to the left of a line with a slope of $y = -0.36x + 40$ meet the second of three criteria for Low-Ca (high-Ti) granite samples. Samples that do not meet the criteria for Low-Ca (high-Ti) granite samples in this step are classified into the Low-Ca granite subgroup.

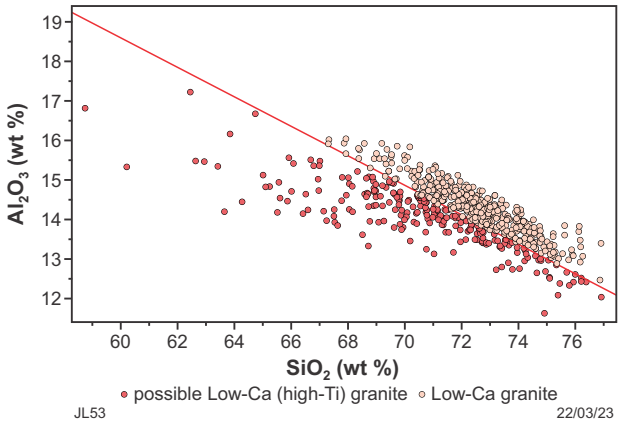

Figure 48. SiO_2 vs Al_2O_3 showing samples that meet the criteria of Step 7.2 for possible Low-Ca (high-Ti) granite and remaining samples that are returned to the Low-Ca granite group

7.3 SiO_2 vs Zr

Samples that meet the criteria for Low-Ca (high-Ti) granite in Steps 7.1 and 7.2 are additionally assessed in Step 7.3. On a plot of SiO_2 wt% vs Zr ppm (Fig. 49), samples that plot above a line with a slope of $y = -10x + 1125$ *or* to the right of a line with a slope of $y = -67.273x + 5277.3$ are classified into the Low-Ca (high-Ti) granite subgroup. Samples that plot to the left of those lines are classified into the Low-Ca granite subgroup.

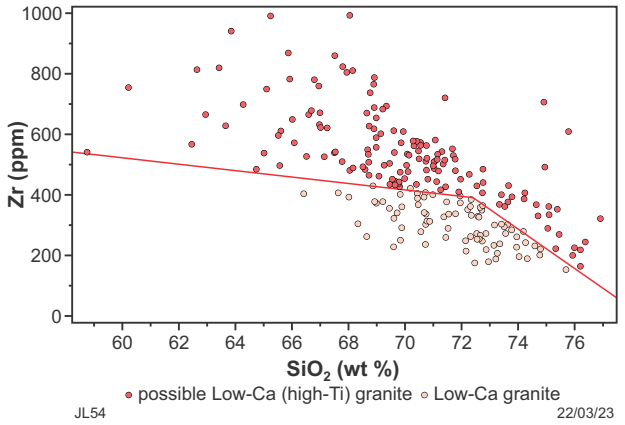

Figure 49. SiO_2 vs Zr showing samples that meet the criteria of Step 7.3 for possible Low-Ca (high-Ti) granite and samples that remain in the Low-Ca granite group

Consolidation of Low-Ca granite calculations

All Low-Ca granite group calculations have been consolidated into a single calculation that is provided in the MS Excel data file (Appendix 1) and the calculation file for ioGAS (Appendix 3). If any sample meets all of the criteria for the Low-Ca granite group (i.e. Steps 4.1–4.9), then the cell in the 'Low-Ca granite group' column will output a value of '1' and the granite classification will be attributed as either 'Low-Ca granite' or 'Low-Ca (high-Ti) granite' (depending on the outcome of Steps 7.1–7.3). Mantle normalized trace element patterns for Low-Ca granites and Low-Ca (high-Ti) granites are shown in Figures 50 and 51 respectively.

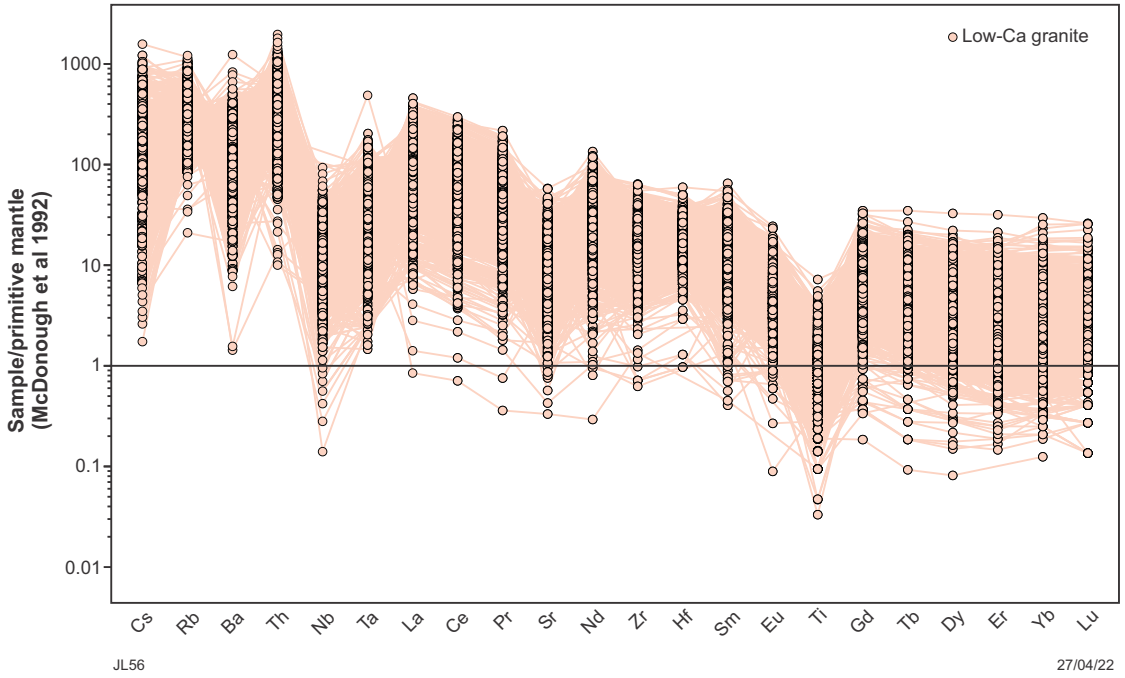

Figure 50. Primitive mantle (McDonough et al., 1992) normalized trace element patterns showing Low-Ca granite samples

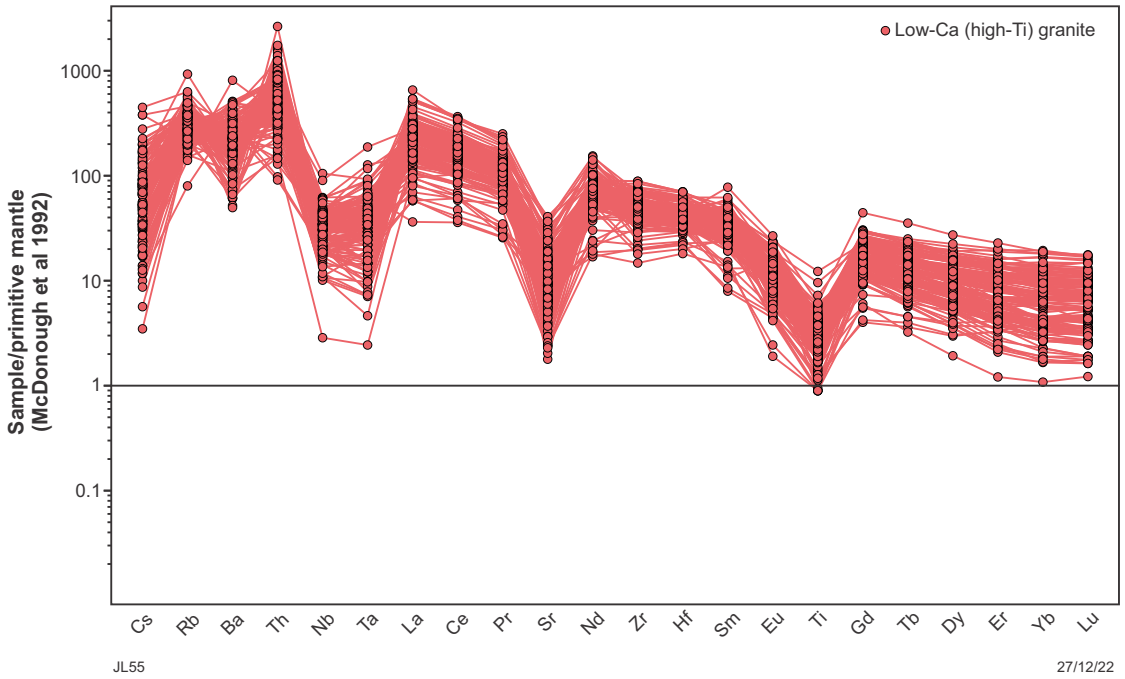

Figure 51. Primitive mantle (McDonough et al., 1992) normalized trace element patterns showing Low-Ca (high-Ti) granite samples

Step 8. Redistributing samples between Low-Ca granite and Mafic granite groups

Samples that classify as 'Low-Ca granite' (i.e. not 'Low-Ca (high-Ti) granite') are additionally assessed on a plot of SiO_2 wt% vs Th ppm (Fig. 52). Samples plotting below a line with a slope of $y = -5x + 370$ are reclassified from Low-Ca granite to the Mafic granite group.

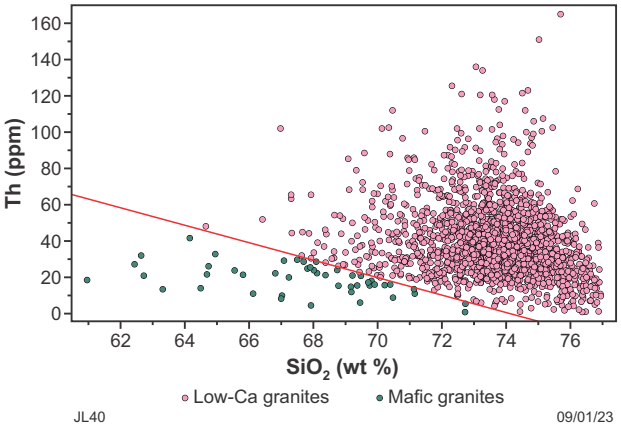

Figure 52. SiO_2 vs Th showing samples that meet Step 8 criteria to be reclassified from Low-Ca granites to Mafic granites

Step 9. Division of Mafic granite group into subgroups

Champion and Sheratons' 'Mafic granite' group is subdivided here based on proxies reflecting how 'primitive' (i.e. mafic or ultramafic) the melt source was (Mg-number and Ni and Cr concentration) and how enriched the source was and/or how deep the source was when melting occurred (Sr/Y). The Mafic granite group are also subdivided based on K_2O/Na_2O, which is interpreted here to mainly relate to the composition of crustal components enriching their mantle sources and/or subsequent mixing with crustal-derived melts of felsic composition (e.g. High-Ca and Low-Ca granitic melts).

9.1 Division based on Sr/Y

Mafic granite group samples are divided based on Sr/Y ratio into 'Sanukitoid and Sanukitoid-like' samples (both high-Sr/Y; ≥30) and Diorite (low-Sr/Y; <30) (Fig. 53).

9.2 Division of high-Sr/Y Mafic granite group samples into Sanukitoid and Sanukitoid-like subgroups

Samples that are classified as 'Sanukitoid and Sanukitoid-like' in Step 9.1 are additionally assessed by Steps 9.2.1, 9.2.2, 9.2.3 and 9.2.4 to determine whether they are Sanukitoid *or* Sanukitoid-like.

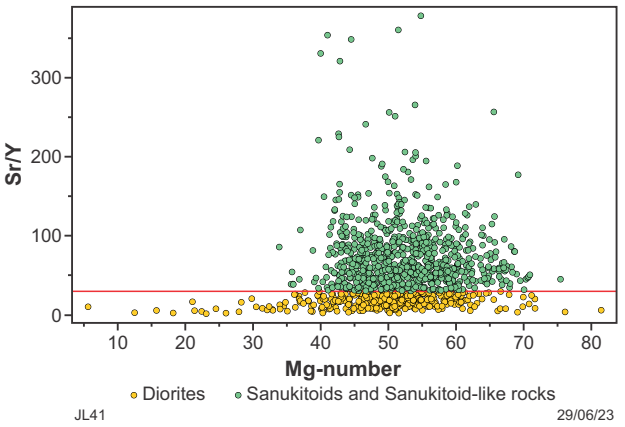

Figure 53. Mg-number vs Sr/Y showing subdivision of Mafic granite group into Sanukitoid or Sanukitoid-like samples (Sr/Y ≥30) and Diorite samples (Sr/Y <30)

9.2.1 Division based on SiO_2 vs Mg-number

On a plot of SiO_2 vs Mg-number (Fig. 54), samples that plot below three lines with slopes of $y = -1.5x + 145$ *or* $y = -1.25x + 130$ *or* $y = -0.8333x + 101.67$ are tentatively classified as Sanukitoid-like, whereas those that plot above these lines are tentatively classified as Sanukitoid.

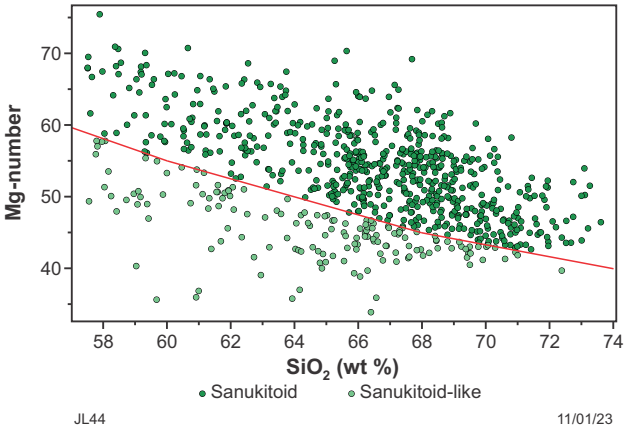

Figure 54. SiO_2 vs Mg-number showing samples that meet the criteria of Step 9.2.1 for Sanukitoid-like and remaining samples that classify as Sanukitoid

9.2.2 Division based on SiO_2 vs Cr

Samples that are classified as Sanukitoid in Step 9.2.1 are reassessed on a plot of SiO_2 wt% vs Cr ppm (Fig. 55). Samples that plot below a line with a slope of $y = -9.0909x + 627.27$ are reclassified as Sanukitoid-like.

9.2.3 Division based on SiO_2 vs Ni

Samples that are classified as Sanukitoid in Steps 9.2.1 and 9.2.2 are reassessed on a plot of SiO_2 wt% vs Ni ppm (Fig. 56). Samples that plot to the left of a line with a slope of $y = 6.25x + 425$ are reclassified as Sanukitoid-like.

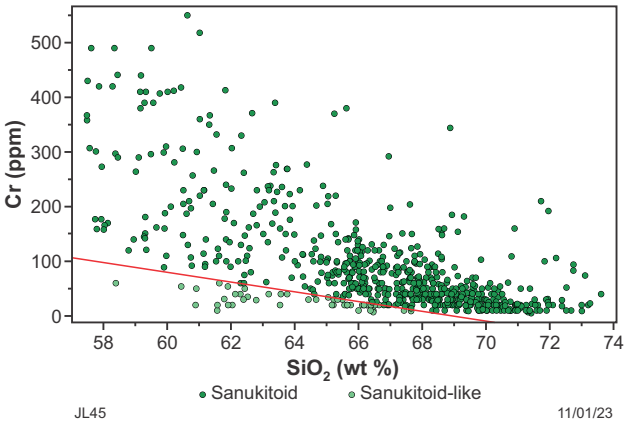

Figure 55. SiO_2 vs Cr showing samples that meet the criteria of Step 9.2.2 for reclassification from the Sanukitoid subgroup to the Sanukitoid-like subgroup and samples that remain within the Sanukitoid subgroup

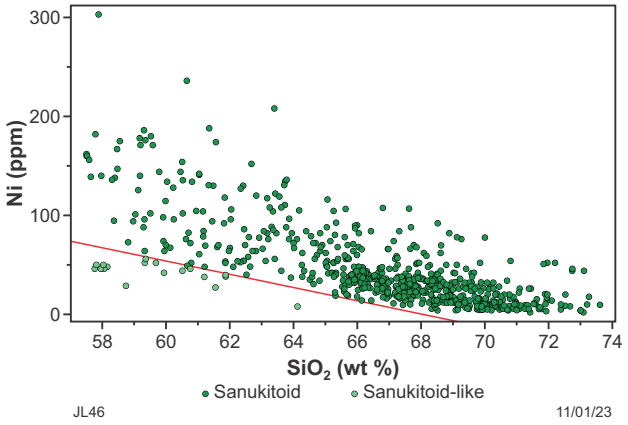

Figure 56. SiO_2 vs Ni showing samples that meet the criteria of Step 9.2.3 for reclassification from the Sanukitoid subgroup to the Sanukitoid-like subgroup and samples that remain within the Sanukitoid subgroup

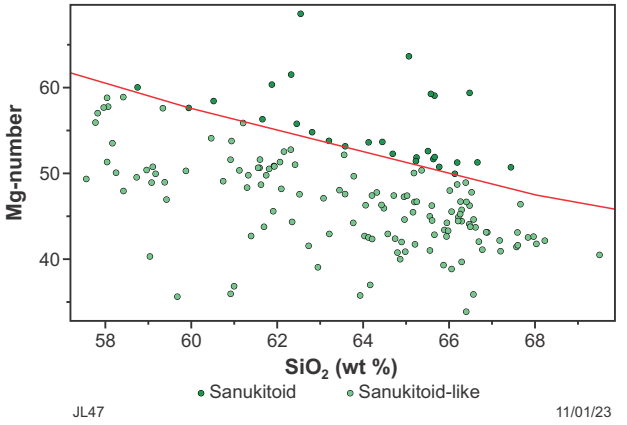

Figure 57. SiO_2 vs Mg-number showing samples that meet the criteria of Step 9.2.4 for reclassification from the Sanukitoid-like subgroup to the Sanukitoid subgroup and samples that remain within the Sanukitoid-like subgroup

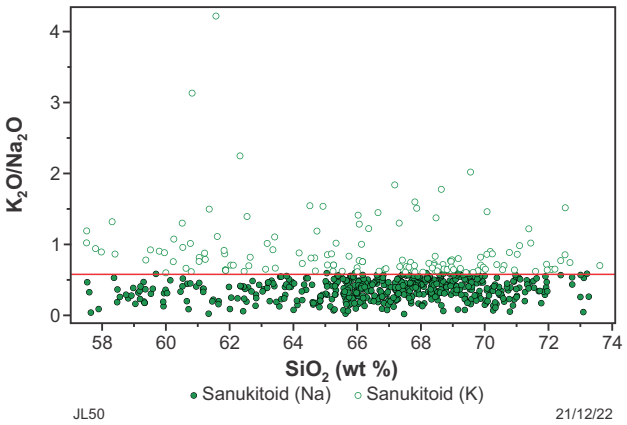

Figure 58. SiO_2 vs K_2O/Na_2O showing samples classified as Sanukitoid further sub-divided based on their K_2O/Na_2O ratios into sodic (Na) and potassic (K) Sanukitoids

9.2.4 Reclassification from Sanukitoid-like to Sanukitoid based on SiO_2 vs Mg-number

Samples that classify as Sanukitoid-like in Steps 9.2.1, 9.2.2 and 9.2.3 are reassessed on a plot of SiO_2 vs Mg-number (Fig. 57). Samples that plot above three lines with slopes of $y = -1.5x + 147.5$ *and* $y = -1.25x + 132.5$ *and* $y = -0.8333x + 104.17$ are reclassified as Sanukitoid, whereas those that plot below these three lines remain classified as Sanukitoid-like.

9.3 Division based on K_2O/Na_2O

Samples that are classified as Sanukitoid, Sanukitoid-like or Diorite are subdivided based on their K_2O/Na_2O ratios into sodic (Na; K_2O/Na_2O <0.6) and potassic (K; K_2O/Na_2O ≥0.6) varieties (Figs 58–60).

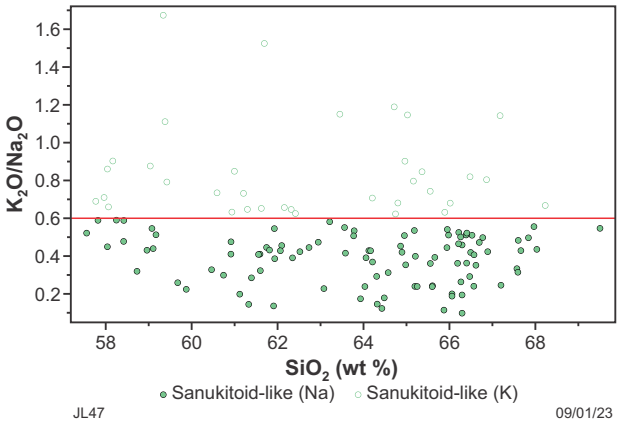

Figure 59. SiO_2 vs K_2O/Na_2O showing samples classified as Sanukitoid-like further sub-divided based on their K_2O/Na_2O ratios into sodic (Na) and potassic (K) Sanukitoid-like samples

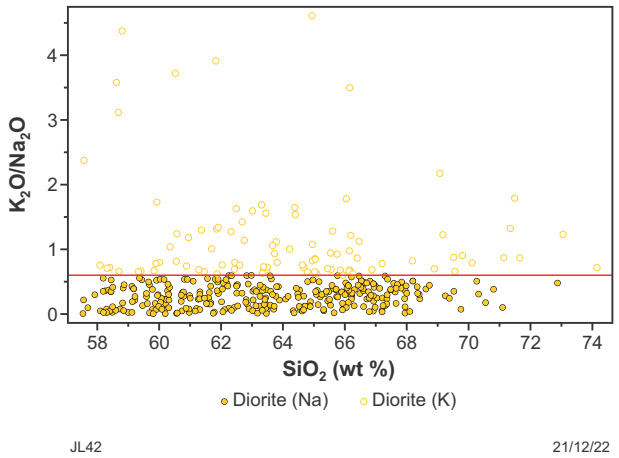

Figure 60. SiO_2 vs K_2O/Na_2O showing samples classified as Diorite further subdivided based on their K_2O/Na_2O ratios into sodic (Na) and potassic (K) Diorites

Consolidation of Mafic granite group calculations

All Mafic granite group calculations have been consolidated into a single calculation that is provided in the MS Excel data file (Appendix 1) and calculation file for ioGAS (Appendix 3). If any sample meets all of the criteria above for the Mafic granite group (i.e. Steps 4, 5 and 8), then the cell in the 'Mafic granite group' column will output a value of '1', and the granite classification will be attributed as either 'Sanukitoid (Na)', 'Sanukitoid (K)', 'Sanukitoid-like (Na)', 'Sanukitoid-like (K)', 'Diorite (Na)' or 'Diorite (K)', depending on the outcome of Steps 9.1–9.3. Mantle normalized trace element patterns for the Mafic granite subgroups are shown in Figures 61–66.

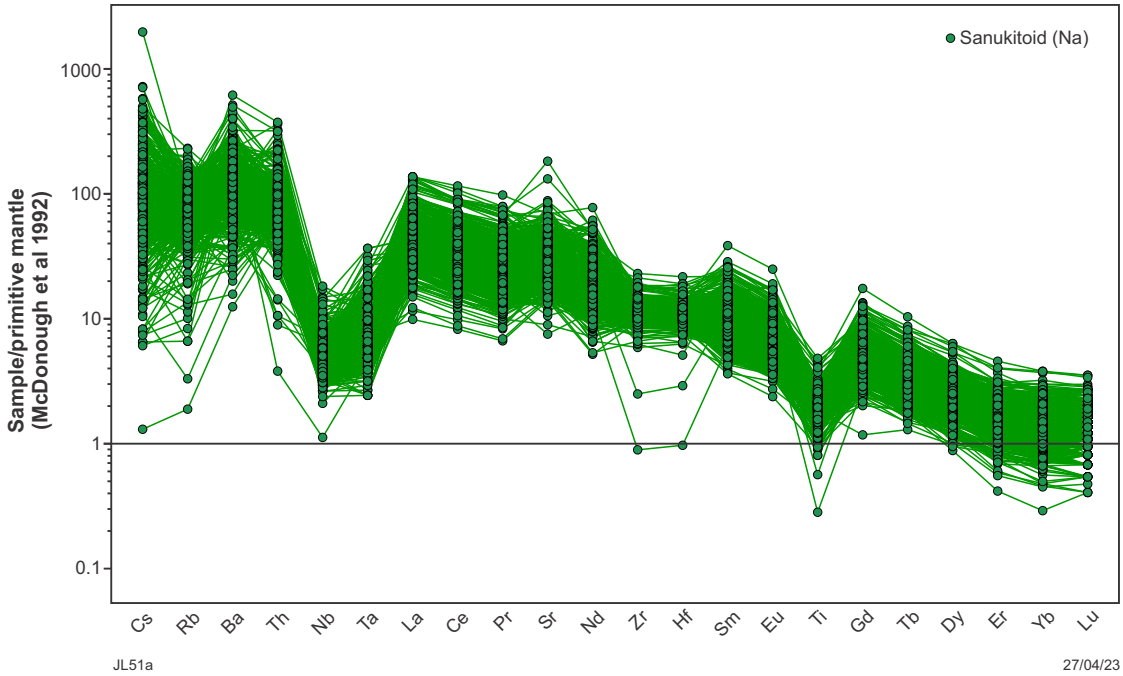

Figure 61. Primitive mantle (McDonough et al., 1992) normalized trace element patterns showing Sanukitoid (Na) samples

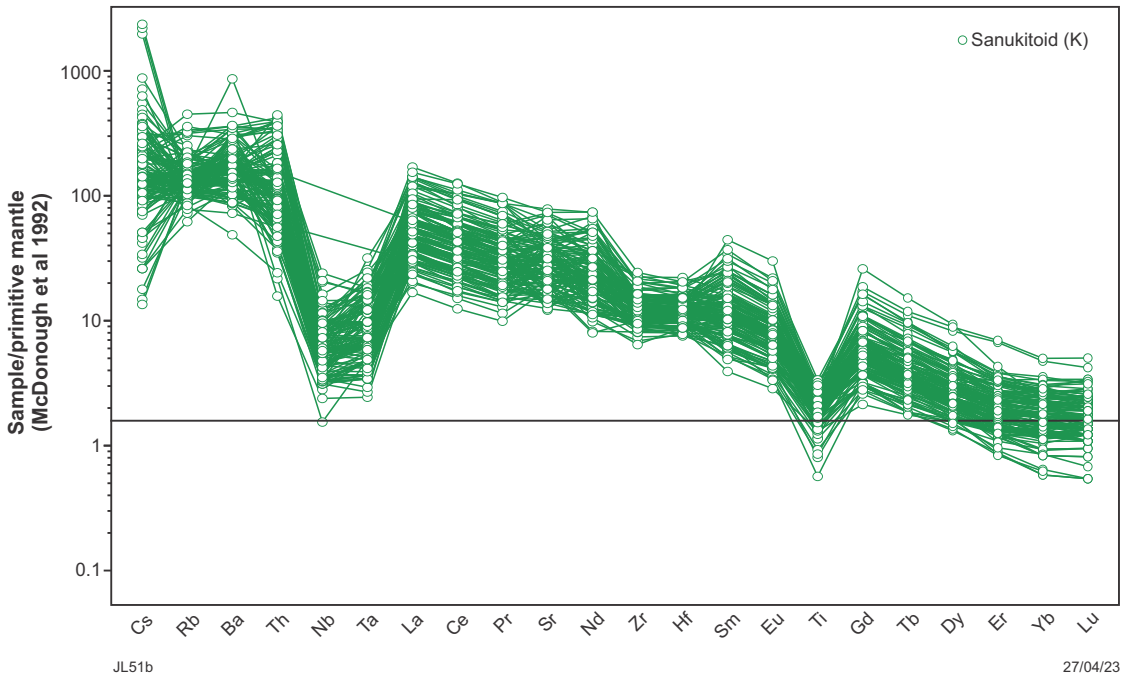

Figure 62. Primitive mantle (McDonough et al., 1992) normalized trace element patterns showing Sanukitoid (K) samples

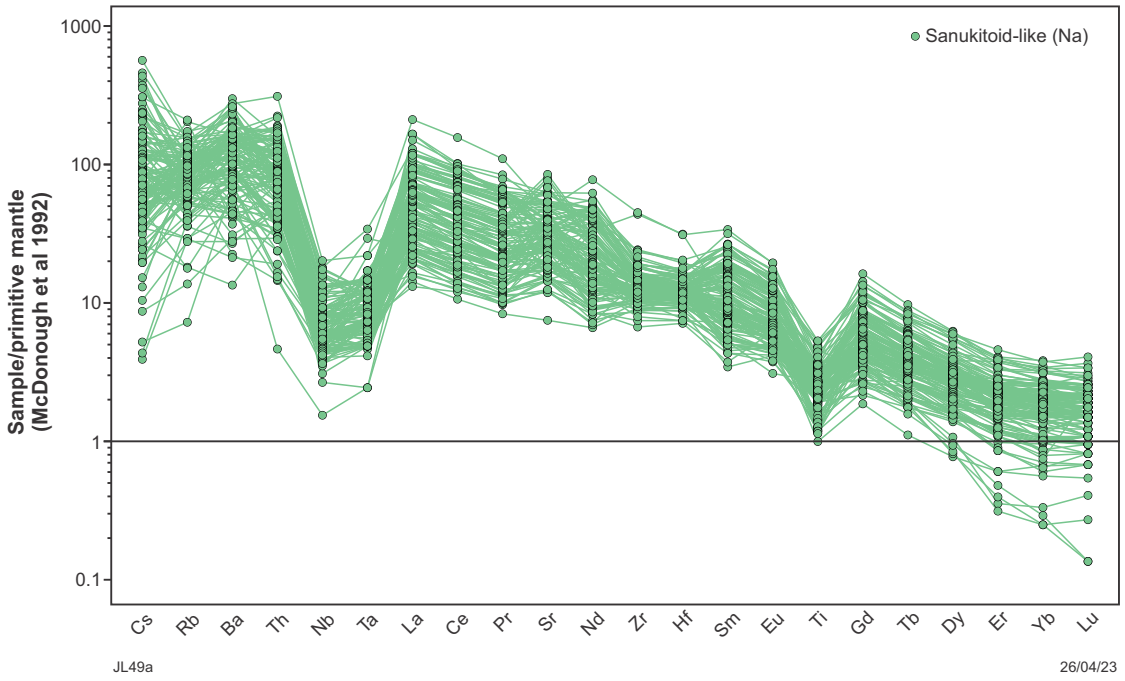

Figure 63. Primitive mantle (McDonough et al., 1992) normalized trace element patterns showing Sanukitoid-like (Na) samples

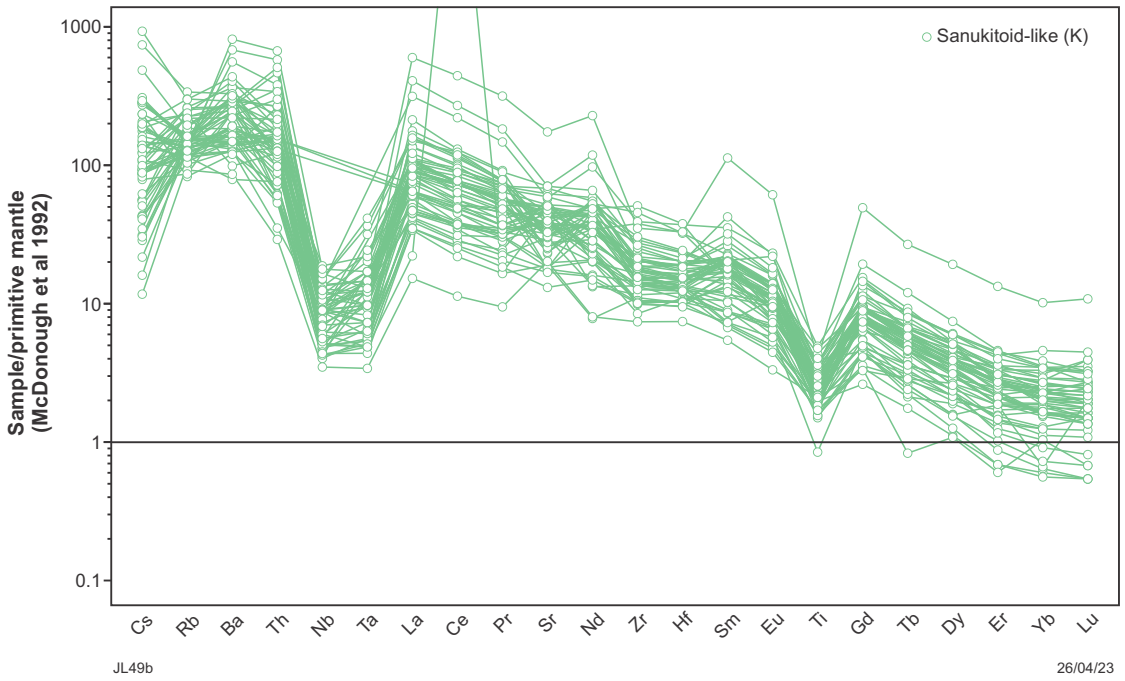

Figure 64. Primitive mantle (McDonough et al., 1992) normalized trace element patterns showing Sanukitoid-like (K) samples

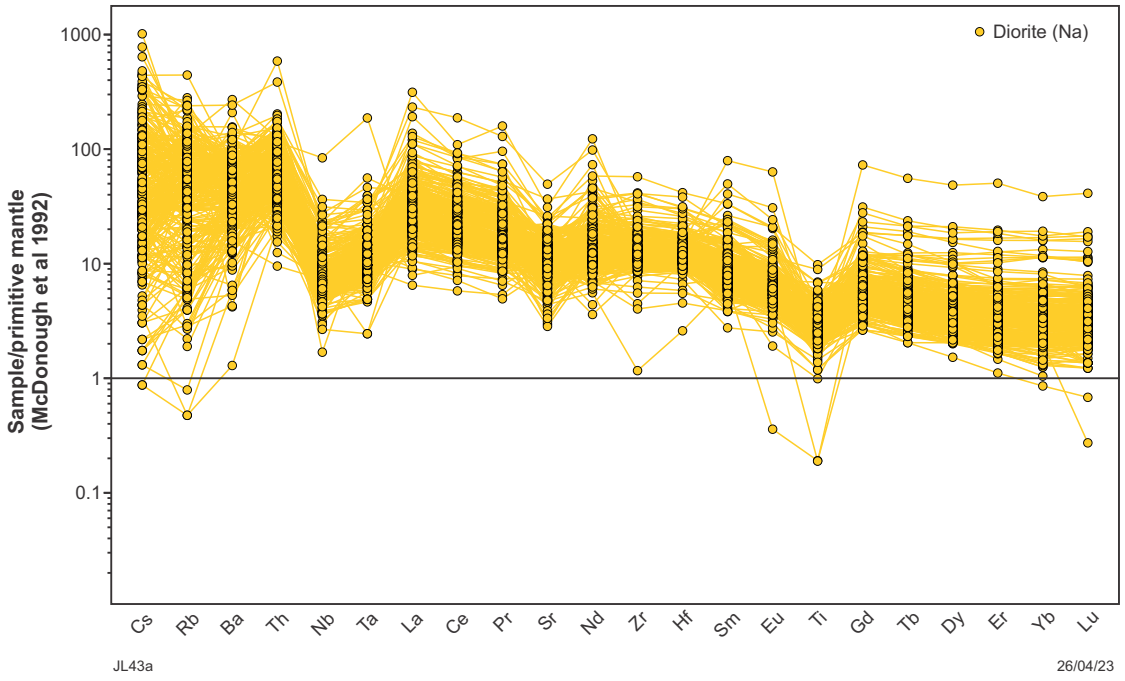

Figure 65. Primitive mantle (McDonough et al., 1992) normalized trace element patterns showing Diorite (Na) samples

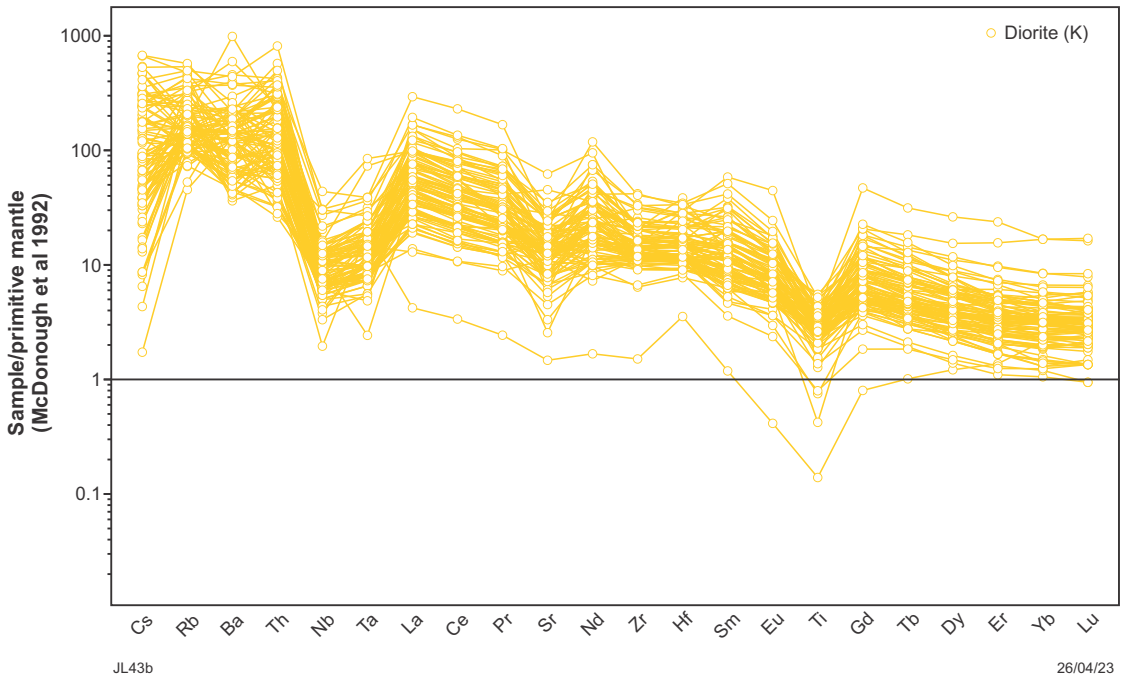

Figure 66. Primitive mantle (McDonough et al., 1992) normalized trace element patterns showing Diorite (K) samples

References

Champion, DC and Cassidy, KF 2002, Chapter 8. An overview of the Yilgarn and its crustal evolution, *in* The characterisation and metallogenic significance of Archaean granitoids of the Yilgarn Craton, Western Australia *edited by* KF Cassidy, DC Champion, NJ McNaughton, IR Fletcher, AJ Whitaker, IV Bastrakova and A Budd: Minerals and Energy Research Institute of Western Australia, MERIWA Project no. M281/AMIRA Project no. 482 (Report No. 222), p. 8.1–8.21 + 9 figures.

Champion, DC and Sheraton, JW 1997, Geochemistry and Nd isotope systematics of Archaean granites of the Eastern Goldfields, Yilgarn Craton, Australia: Implications for crustal growth processes: Precambrian Research, v. 83, no. 1–3, p. 109–132, doi:10.1016/S0301-9268(97)00007-7.

Lowrey, JR, Smithies, RH and Champion, DC 2022, Yilgarn granite project – notes to accompany 2022 data release: Geological Survey of Western Australia, Record 2022/9, 3p.

Martin, H, Smithies, RH, Rapp, R, Moyen, J-F and Champion, DC 2005, An overview of adakite, tonalite–trondhjemite–granodiorite (TTG), and sanukitoid: Relationships and some implications for crustal evolution: Lithos, v. 79, p. 1–24, doi:10.1016/j.lithos.2004.04.048.

McDonough, WF, Sun, S-S, Ringwood, AE, Jagoutz, E and Hofmann, AW 1992, Potassium, rubidium, and cesium in the Earth and Moon and the evolution of the mantle of the Earth: Geochimica et Cosmochimica Acta, v. 56, no. 3, p. 1001–1012, doi:10.1016/0016-7037(92)90043-I.

Moyen, J-F and Martin, H 2012, Forty years of TTG research: Lithos, v. 148, p. 312–336, doi:10.1016/j.lithos.2012.06.010.

Shand, SJ 1922, The problem of the alkaline rocks: Proceedings of the Geological Society of South Africa, v. 25, p. xix–xxxiii.

Shirey, SB and Hanson, GN 1984, Mantle-derived Archaean monozodiorites and trachyandesites: Nature, v. 310, p. 222–224.

Smithies, RH, Lu, Y, Gessner, K, Wingate, MTD and Champion, DC 2018, Geochemistry of Archean granitic rocks in the South West Terrane of the Yilgarn Craton: Geological Survey of Western Australia, Record 2018/10, 13p.

Smithies, RH, Lu, Y, Lowrey, JR, Ivanic, TJ, Champion, DC and Wilde, SA 2021, Variations in granite geochemistry in the southwest Yilgarn, *in* Accelerated Geoscience Program extended abstracts *compiled by* Geological Survey of Western Australia: Geological Survey of Western Australia Record 2021/4, p. 149–153.

Stanley, CR and Lawie, D 2007, Average relative error in geochemical determinations: Clarification, calculation, and a plea for consistency: Exploration and Mining Geology, v. 16, p. 267–275.

Stern, RA, Hanson, GN and Shirey, SB 1989, Petrogenesis of mantle-derived, LILE-enriched Archean monzodiorites and trachyandesites (sanukitoids) in southwestern Superior Province: Canadian Journal of Earth Sciences, v. 26, p. 1688–1712.

RECORD 2023/12

SYSTEMATIC CLASSIFICATION OF YILGARN CRATON GRANITIC ROCKS

JR Lowrey, RH Smithies, DC Champion and KF Cassidy

Access GSWA products

All products
All GSWA products are free to download as PDFs from the DMIRS eBookshop <www.dmirs.wa.gov.au/ebookshop>.
View other geoscience information on our website <www.dmirs.wa.gov.au/gswa>.

Hard copies
Limited products are available to purchase as hard copies from the First Floor Counter at Mineral House or via the DMIRS eBookshop <www.dmirs.wa.gov.au/ebookshop>.

Fieldnotes
Fieldnotes is a free digital-only quarterly newsletter which provides regular updates to the State's exploration industry and geoscientists about GSWA's latest programs, products and services.
Access by subscribing to the GSWA eNewsletter <www.dmirs.wa.gov.au/gswaenewsletter> or downloading the free PDF from the DMIRS eBookshop <www.dmirs.wa.gov.au/ebookshop>.

GSWA eNewsletter
The GSWA eNewsletter is an online newsletter that contains information on workshops, field trips, training and other events.
To keep informed, please subscribe <www.dmirs.wa.gov.au/gswaenewsletter>.

Further details of geoscience products are available from:

First Floor Counter
Department of Mines, Industry Regulation and Safety
100 Plain Street
EAST PERTH WESTERN AUSTRALIA 6004
Phone: +61 8 9222 3459 Email: publications@dmirs.wa.gov.au
www.dmirs.wa.gov.au/GSWApublications